FINITE ELEMENT SIMULATION OF CRACK PROPAGATION FOR STEEL FIBER REINFORCED CONCRETE

A THESIS SUBMITTED TO
THE GRADUATE SCHOOL OF CIVIL ENGINEERING
OF
MIDDLE EAST TECHNICAL UNIVERSITY

BY

KAAN ÖZENÇ

IN PARTIAL FULFILLMENT OF THE REQUIREMENTS
FOR
THE DEGREE OF MASTER OF SCIENCE
IN
CIVIL ENGINEERING

JULY 2009

Approval of the thesis:

FINITE ELEMENT SIMULATION OF CRACK PROPAGATION FOR STEEL FIBER REINFORCED CONCRETE

submitted by **KAAN ÖZENÇ** in partial fulfillment of the requirements for the degree of **Master of Science in Civil Engineering Department, Middle East Technical University** by,

Prof. Dr. Canan Özgen _____
Dean, Graduate School of **Natural and Applied Sciences**

Güney Özcebe _____
Head of Department, **Civil Engineering**

Assoc. Prof. Dr. İsmail Özgür Yaman _____
Supervisor, **Civil Engineering Department, METU**

Assoc. Prof. Dr. Serkan Dağ _____
Co-supervisor, **Mechanical Engineering Department, METU**

Examining Committee Members:

Prof. Dr. Mustafa Tokyay
Civil Engineering, METU _____

Assoc. Prof. Dr. İsmail Özgür Yaman
Civil Engineering, METU _____

Assoc. Prof. Dr. Serkan Dağ
Mechanical Engineering, METU _____

Assoc. Prof. Dr. Barış Binici
Civil Engineering, METU _____

Asst.Prof.Dr. Sinan Turhan Erdogan
Civil Engineering, METU _____

Date: _____

I hereby declare that all information in this document has been obtained and presented in accordance with academic rules and ethical conduct. I also declare that, as required by these rules and conduct, I have fully cited and referenced all material and results that are not original to this work.

Name, Last Name: KAAN ÖZENÇ

Signature :

ABSTRACT

FINITE ELEMENT SIMULATION OF CRACK PROPAGATION FOR STEEL FIBER REINFORCED CONCRETE

Özenç, Kaan
M.S., Department of Civil Engineering
Supervisor : Assoc. Prof. Dr. İsmail Özgür Yaman
Co-Supervisor : Assoc. Prof. Dr. Serkan Dağ

July 2009, 90 pages

Steel fibers or fibers in general are utilized in concrete to control the tensile cracking and to increase its toughness. In literature, the effects of fiber geometry, mechanical properties, and volume on the properties of fiber reinforced concrete have often been experimentally investigated by numerous studies. Those experiments have shown that useful improvements in the mechanical behavior of brittle concrete are achieved by incorporating steel fibers. This study proposes a simulation platform to determine the influence of fibers on crack propagation and fracture behavior of fiber reinforced concrete. For this purpose, a finite element (FE) simulation tool is developed for the fracture process of fiber reinforced concrete beam specimens subjected to flexural bending test.

Within this context, the objective of this study is twofold. The first one is to investigate the effects of finite element mesh size and element type on stress intensity factor (SIF) calculation through finite element analysis. The second objective is to develop a simulation of the fracture process of fiber reinforced concrete beam specimens.

The properties of the materials, obtained from literature, and the numerical simulation procedure, will be explained. The effect of fibers on SIF is included by unidirectional elements with nonlinear generalized force-deflection capability. Distributions and orientation of fibers and possibility of anchorage failure are also added to simulation.

As a result of this study it was observed that with the adopted simulation tool, the load-deflection relation obtained by experimental studies is predicted reasonably.

Keywords: Concrete, steel fiber, finite element, fracture mechanics, crack propagation

ÖZ

SONLU ELEMANLAR YÖNTEMİYLE ÇELİK LİFLİ BETONDA ÇATLAK İLERLEME SİMÜLASYONU

Özenç, Kaan
Yüksek Lisans, İnşaat Mühendisliği Bölümü
Tez Yöneticisi : Doç. Dr. İsmail Özgür Yaman
Ortak Tez Yöneticisi : Doç. Dr. Serkan Dağ

Temmuz 2009, 90 sayfa

Çelik veya diğer çeşit lifler, betonun çekme çatlaklarını kontrol etmek ve betonun tokluğunu artırmak için kullanılır. Çelik liflerin geometrilerinin, miktarlarının ve mekanik özelliklerinin çelik lifli beton üzerindeki etkisi sayısız çalışmayla incelenmiştir. Bu çalışmalar fiberlerin betonda kullanılmasının betonun mekanik özelliklerine olumlu etki ettiklerini göstermiştir. Bu çalışma fiberlerin çatlak ilerleyişine etkisini ve çelik lifli betonun kırılma davranışını tanımlayan bir simülasyon platformu önermektedir. Bu amaçla, eğilme testi altındaki çelik lifli betonun kırılma ilerleyişi için sonlu elemanlar simülasyonu geliştirilmiştir.

Bu bağlamda, bu çalışmanın amacı iki kategoriye ayrılmıştır. Birincisi, sonlu elemanlar yönteminde kullanılan örgü (mesh) büyüklüğünün ve sonlu eleman özelliklerinin kırılma tokluğu çarpanı üzerindeki etkisinin incelenmesidir. İkinci amaç ise çelik lifli beton kirişlerin kırılma ilerleyişi için bir simülasyon geliştirilmesidir.

Malzeme özellikleri daha önceki deneysel çalışmalardan elde edilen yayınlardan alınmıştır. Liflerin kırılma tokluğu çarpanı üzerindeki etkisi tek yönlü doğrusal olmayan eleman-

lar kullanılarak ve yük-deplasman (yer değiştirme) kapasiteleri göz önüne alınarak simülasyona dahil edilmiştir. Ayrıca liflerin dağılım ve sıyrılma olasılıkları da istatistiksel olarak simülasyona dâhil edilmiştir.

Bu çalışmanın sonucunda uyarlanmış simülasyon aracı kullanılarak elde edilen verilerin yük-deplasman ilişkisi açısından deneysel çalışmalardan elde edilen verilerle kabul edilebilir ölçüde uyuştuğu gözlenmiştir.

Anahtar Kelimeler: Beton, çelik lif, sonlu elemanlar, kırılma mekaniği, çatlak ilerleyişi

ACKNOWLEDGMENTS

This thesis was conducted under the supervision of Assoc. Prof. Dr. İsmail Özgür Yaman and Assoc. Prof. Dr. Serkan Dağ. I would like to express my sincere appreciation for the support, encouragement, guidance and insight they have provided throughout the thesis.

TABLE OF CONTENTS

PLAGIARISM iii
ABSTRACT iv
ÖZ vi
ACKNOWLEDGMENTS viii
TABLE OF CONTENTS ix
LIST OF FIGURES xi
LIST OF TABLES xiii
CHAPTERS
1 INTRODUCTION 1
1.1 History of Fracture Mechanics 1
1.2 Objectives 2
1.3 Scope 3
2 LITERATURE REVIEW AND BACKGROUND 5
2.1 Introduction to Fracture Mechanics 5
2.2 General Principles of Linear Elastic Fracture Mechanics (LEFM) Approach 7
2.2.1 Stress Analysis Approach 7
2.2.2 Energy Analysis Approach 15
2.2.3 Relationship between Stress Intensity Factor & Energy Release Rate 18
2.3 General Principles of Nonlinear Elastic Fracture Mechanics (NLEFM) Approach 19
2.4 Fracture Mechanics of Concrete 24
2.4.1 Fictitious Crack Approach 24
2.4.2 Effective-Elastic Crack Approach 28
2.5 Finite Element Analysis of Fracture Mechanics Properties 34
2.5.1 Finite Element Modeling of Singularities 34

2.5.2 Calculation of Stress Intensity Factor Using Finite Element Method 38
2.5.3 The Main Feature and Hypothesis of Finite Element Analysis of Fracture in Concrete 41
3 INTRINSIC PARAMETERS OF FINITE ELEMENT ANALYSIS OF FRACTURE 47
3.1 The Issue of Stability of Crack Propagation 47
3.2 Finite Element Size and Types of Elements 50
4 CRACK PROPAGATION SIMULATION FOR STEEL FIBER REINFORCED CONCRETE 57
4.1 Material Properties and Finite Element Types. 57
4.2 Fiber Orientation Factor 62
4.3 Possibility of Pull Out 64
4.4 Finite Element Analysis 65
5 SUMMARY AND CONCLUSIONS 72
5.1 Summary 72
5.2 Conclusions 72
5.3 Recommendations for Future Studies 73
REFERENCE 75
APPENDIX A 79

LIST OF FIGURES

FIGURES

Figure 2.1 Mode types of crack propagation. 5
Figure 2.2 Stress-strain responses of common materials. 6
Figure 2.3 Stress components on a infinitesimal cube. 7
Figure 2.4 Definition of the coordinate axis ahead of a crack tip. The z direction is normal to the page 14
Figure 2.5 Infinite plate with crack subjected to tension 17
Figure 2.6 Schematic view of R-curve. 21
Figure 2.7 J-Integral contour. 22
Figure 2.8 Plastic zone in inelastic materials. 23
Figure 2.9 A cohesive crack with partially separated crack surface. 25
Figure 2.10 Complete tensile stress-elongation curve for fictitious crack model by Hillerborg 26
Figure 2.11 A micro crack band model and stress strain curve for crack band model 27
Figure 2.12 Elastic and plastic fracture responses and loading and unloading procedure 29
Figure 2.13 Series of geometrically similar three-point bending test structures. 31
Figure 2.14 Three-node bar element 35
Figure 2.15 Linear interpolation shape functions for 3-node bar elements 36
Figure 2.16 Singular elements at the crack tip and nodes used in calculation of SIFs. 37
Figure 2.17 Crack Front and the Local Coordinate System. 39
Figure 2.18 Deformed Crack Surface. 39
Figure 2.19 Cohesive crack model and damage zone in concrete. 43
Figure 2.20 Finite element view of discrete crack model. 43
Figure 2.21 Finite element analysis of three-point bending beam. 44

Figure 2.22 General review of stress distribution in fictitious crack model 45
Figure 2.23 Triaxial stresses in the FPZ and its nonlocal behavior in reinforced concrete. 46
Figure 3.1 Mesh refinements with 20, 40, and 80 elements at fracture face 48
Figure 3.2. Dimensionless load versus midpoint deflection curves for beams analyzed by Carpinteri 49
Figure 3.3 4-node “plane42” elements of ANSYS. 51
Figure 3.4 High order 8-node “plane82” elements of ANSYS 51
Figure 3.5 Mesh resolutions of three-point bending specimen. 51
Figure 3.6 Relationship between SIF and thickness. 53
Figure 3.7 Three-point bending test procedure. 53
Figure 4.1 Experimental three-point bending test beam 58
Figure 4.2 Gopalaratnam and Shah’s strain softening model 58
Figure 4.3 Pull out experiment of steel fibers 60
Figure 4.4 Slip-Load curve for crimped-shape steel fiber 61
Figure 4.5 Behavior and inputs for COMBIN39 type of element. 61
Figure 4.6 Orientation factor with various cross-sectional dimensions. 63
Figure 4.7 Different conditions with four boundaries 63
Figure 4.8 Probability of pull out failure 65
Figure 4.9 Flow chart for fracture process testing of steel fiber reinforced concrete. 66
Figure 4.10 Crack Propagation Steps. 67
Figure 4.11 Load–deflection curves for fiber reinforced concrete beams V_f = 1.0 69
Figure 4.12 Load–deflection curves for fiber reinforced concrete beams V_f = 1.5 69
Figure 4.13 Load–deflection curve for fiber reinforced concretes and plain concrete 70
Figure 4.14 Load–deflection curve for various fiber contents. 71
Figure A.1 Mesh resolution according to 10 elements at fracture surface. 79
Figure A.2 Mesh resolution according to 20 elements at fracture surface. 81
Figure A.3 Mesh resolution according to 40 elements at fracture surface. 83
Figure A.4 Mesh resolution according to 13 elements at fracture surface. 85
Figure A.5 Mesh resolution according to 23 elements at fracture surface. 87
Figure A.6 Mesh resolution according to 43 elements at fracture surface. 89

LIST OF TABLES

TABLES

Table 3.1 The properties of beams analyzed by Carpinteri. 48
Table 3.2 Impact of mesh size on SIF calculations with 4-node elements. 55
Table 3.3 Impact of mesh size on SIF calculations with 8-node high-order elements. 56

CHAPTER 1

INTRODUCTION

1.1 History of Fracture Mechanics

The field of fracture mechanics has focused on the estimation and prevention of fracture as a scientific discipline since the middle of the 20th century. In 1921, Griffith attempted to explain the large difference between the theoretical and measured tensile strength of glass. He attributed the large discrepancies to high stresses in the neighborhood of micro cracks and developed a theory of brittle failure based on fracture mechanics.

The study of fracture mechanics of concrete originated in 1961 with Kaplan (Kaplan, 1961). A very different fracture mechanics theory is needed for concrete compared to that of homogeneous structural materials and Kesler et al. concluded in 1972 that classical linear elastic fracture mechanics was inapplicable to concrete (Kesler et al., 1972). At least two fracture parameters are needed. In 1976, development of the crack band model was recognized by Bažant in which the fracture properties are characterized by the simple slope of the post peak strain softening tied to a certain characteristic width of the crack band front (Bažant, 1976).

A major improvement was made by Hillerborg et al. who introduced the fictitious crack model to concrete, in which the initial slope of the softening area under the stress–separation curve, together with the tensile strength, implies two fracture parameters of the material (Hillerborg et al., 1976). Two parameters were subsequently used in Jenq and Shah's "two-parameter model" (Jenq and Shah, 1985). Similarly, Karihaloo and Nallathambi used two parameters in their "effective crack model" (Karihaloo and Nallathambi, 1989).

The most important attribute of fracture mechanics of concrete is the size effect. Although it was widely believed until the mid-1980s that all the size effects were of statistical origin, and should therefore be relegated to statisticians, in 1969 Leicester suggested that the size effect may originate from fracture mechanics of concrete. Failures caused by fracture were numerically simulated with the crack band model and were described in 1984 by Bažant by a simple size effect formula (Bažant, 1984).

Parallel analysis showed that the fracture model based on the size effect law by Bažant and the Jenq–Shah's "two parameter model" results in about the same size effect and, therefore, are approximately equivalent. Likewise, Karihaloo and Nallathambi's model was shown to be approximately equivalent to "two parameter model", and thus to the size effect model.

Steel fibers or fibers in general are utilized in concrete to increase its toughness and load-carrying capacity after cracking. In literature, the effects of fiber geometry, mechanical properties, and volume on the properties of fiber reinforced concrete have often been experimentally investigated. The mechanical response of fiber reinforced concrete is thoroughly influenced by fiber-matrix interface, which is usually evaluated by a pullout test of fibers. This study proposes a simulation platform to determine the influence of fibers on crack propagation and fracture behavior of fiber reinforced concrete.

1.2 Objectives

The goal of this thesis is to develop a finite element simulation tool for the fracture process of fiber reinforced concrete beam specimens subjected to flexural bending test. Within this context, the object of this study is twofold. The first one is to investigate the effects of finite element mesh size and element type on stress intensity factor (SIF) calculation through finite element analysis. After determining the effects of mesh size and element type, the second objective is the simulation of the fracture

process of fiber reinforced concrete beam specimens. The concrete is modeled as a homogenous linearly elastic material. The pull out behavior of the fibers is modeled as link elements with nonlinear properties obtained from literature. During the FE analysis, critical SIF is used as a crack propagation criterion.

1.3 Scope

Experiments have showed that useful improvements in the mechanical behavior of brittle concrete are achieved by incorporating steel fibers. Numerous approaches have been developed to simulate experimental tests via numerical models. This study will investigate a simulation platform to determine the influence of fibers on crack propagation and fracture behavior of concrete. For this purpose, fracture behavior process will be simulated with the finite element method (FEM).

This thesis consists of five chapters. Chapter 2, Literature Review and Background, provides the brief foundations of the present study. Within this context the procedures of the two analyses, namely the approach of stress and energy analyses, of linear elastic fracture mechanics (LEFM) are described. After LEFM, general principles of nonlinear elastic fracture mechanics (NLEFM) are taken into consideration. Later, the concepts related to fracture mechanics of concrete are covered. Finally, in the last section of this chapter, subjects related to finite element applications of fracture mechanics are briefly explained.

In Chapter 3, the efficiency of meshing and element type is thoroughly investigated by comparing finite element solutions and hand book calculations of stress intensity factor.

In Chapter 4, Analytical Study of Crack Propagation of Steel Fiber Reinforced Concrete, the probability work for steel fibers' orientation and pull out properties are identified. The foundations of steel fiber models for the FE simulations are also built

in this chapter. Finally, the analysis of a fiber reinforced concrete beam is performed and the obtained results are compared to experimental tests.

In the final chapter, the findings of the research whose goals have been mentioned in the initial chapter are stated and comments on prospective studies are presented.

CHAPTER 2

LITERATURE REVIEW AND BACKGROUND

2.1 Introduction to Fracture Mechanics

As mentioned in the previous chapter, going back to the mid 20th century, George R. Irwin and his co-workers developed a new fracture theory. Irwin's generalization of the Griffith argument for an energy-related fracture criterion provided a more comprehensive theory of fracture. With this generalized theory, Irwin described the terms *G* (energy absorbed by unit crack progress) and *K* (stress intensity factor) which are used in fracture mechanics to predict the stress intensity near the tip of a crack caused by a remote load or residual stresses more accurately. The underlying idea is that when the stress state in a crack tip becomes critical, a small crack grows and the material fails. Additionally, crack types are categorized by load types as Mode-I, Mode-II, and Mode–III, as shown in Figure 2.1

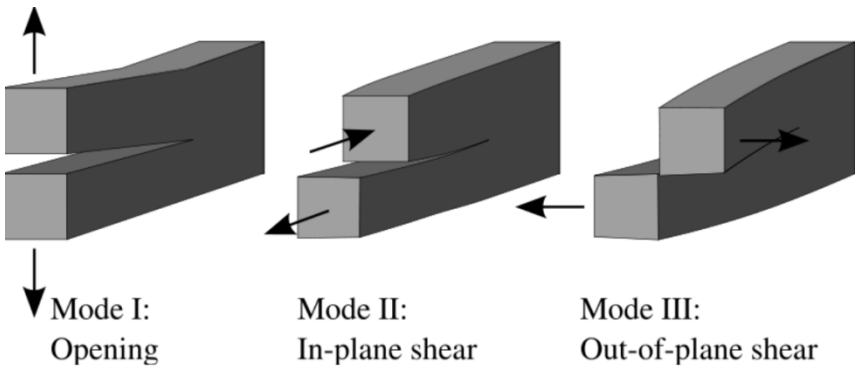

Figure 2.1 Mode types of crack propagation.

Mode-I is an opening mode where the crack surfaces move apart because of a tensile load. Mode-II is a sliding mode where crack surfaces slide over one another in a direction perpendicular to the edge of crack. Mode-III is a tearing mode where the crack surfaces move relative to one another and parallel to the edge of crack (Sanforld, 2002). Since a Mode-I type of crack is the most common type in engineering applications, in this study, only Mode-I is investigated.

The fracture behavior of materials is attributed to their stress (σ) versus strain (ε) responses. Figure 2.2 shows typical $\sigma - \varepsilon$ plots for various idealized materials. In order to analyze the fracture behavior of these materials, the two types of analysis procedures have been developed; linear elastic fracture mechanics (LEFM) and non-linear elastic fracture mechanics (NLEFM). The main difference between the two procedures is that in the first one any propagation of crack leads to a catastrophic failure whereas in the latter one, crack may propagate until it reaches a critical length or critical energy. This chapter briefly describes the analysis procedures for these two LEFM and NLEFM concepts.

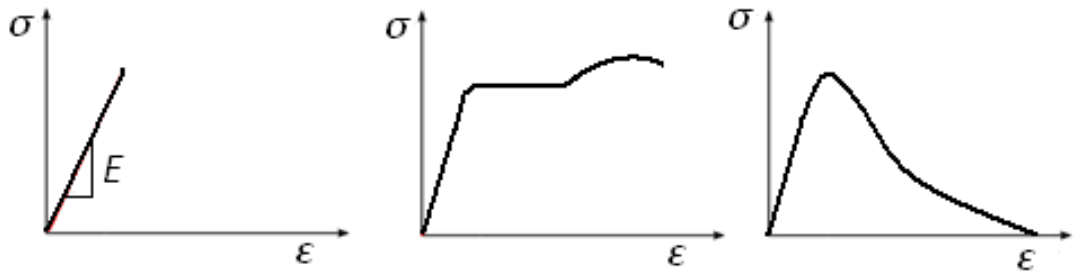

a) Linear elastic (Carbon fiber) b) Elastic-plastic (Mild-steel) c) Quasi-brittle materials (Concrete)

Figure 2.2 Stress-strain responses of common materials.

2.2 General Principles of Linear Elastic Fracture Mechanics (LEFM) Approach

2.2.1 Stress Analysis Approach

In order to introduce the linear elastic fracture mechanics concept, there arises a need for the introduction of the concept of general linear stress and strain relationship. Stress components at any point on a stressed body, σ_x, σ_z, σ_z, τ_{xy}, τ_{xz}, τ_{yz} are defined as shown in Figure 2.3. The nine stress components depicted in Figure 2.3 can be written in matrix form:

$$\sigma_{ij} = \begin{pmatrix} \sigma_x & \tau_{xy} & \tau_{xz} \\ \tau_{yx} & \sigma_y & \tau_{yz} \\ \tau_{zx} & \tau_{zy} & \sigma_z \end{pmatrix} \tag{2.1}$$

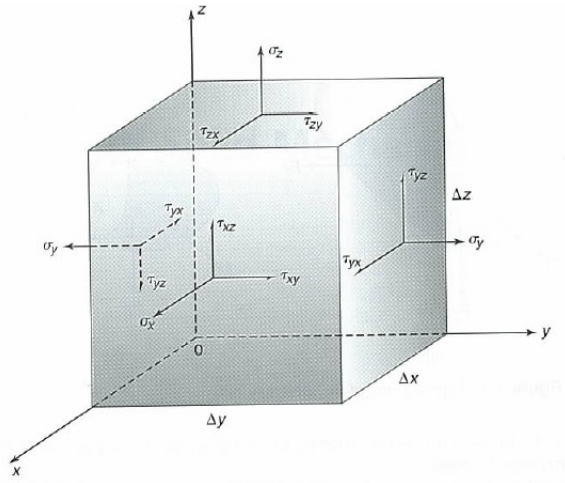

Figure 2.3 Stress components on a infinitesimal cube (Sanforld, 2002).

It can be shown that the moment equilibrium about the centroid of sub domain leads to:

$$\tau_{xy} = \tau_{yx} \quad \tau_{xz} = \tau_{zx} \quad \tau_{yz} = \tau_{zy} \tag{2.2}$$

For the same body, the strain components are related to the displacement components of the body as:

$$\varepsilon_x = \frac{\partial u}{\partial x}$$
$$\varepsilon_y = \frac{\partial v}{\partial y} \tag{2.3}$$
$$\varepsilon_z = \frac{\partial w}{\partial z}$$

$$\gamma_{xy} = \frac{\partial v}{\partial x} + \frac{\partial u}{\partial y}$$
$$\gamma_{xz} = \frac{\partial w}{\partial x} + \frac{\partial u}{\partial z} \tag{2.4}$$
$$\gamma_{yz} = \frac{\partial w}{\partial y} + \frac{\partial v}{\partial z}$$

where u, v, w are the displacements in the coordinate directions x, y, z respectively. The strain components can also be assembled in matrix form as presented in Equation 2.5:

$$\varepsilon_{ij} = \begin{pmatrix} \varepsilon_x & \frac{\gamma_{xy}}{2} & \frac{\gamma_{xz}}{2} \\ \frac{\gamma_{xy}}{2} & \varepsilon_y & \frac{\gamma_{yz}}{2} \\ \frac{\gamma_{xz}}{2} & \frac{\gamma_{yz}}{2} & \varepsilon_z \end{pmatrix} \tag{2.5}$$

When the generalized Hooke's law is employed to model linear elastic and isotropic materials, in the three-dimensional Cartesian coordinate system, the relationship between stress and strain has the form:

$$\varepsilon_x = \frac{1}{E}\left[\sigma_x - \upsilon\left(\sigma_y + \sigma_z\right)\right]$$
$$\varepsilon_y = \frac{1}{E}\left[\sigma_y - \upsilon\left(\sigma_x + \sigma_z\right)\right] \tag{2.6}$$
$$\varepsilon_z = \frac{1}{E}\left[\sigma_z - \upsilon\left(\sigma_x + \sigma_y\right)\right]$$

$$\gamma_{xy} = \frac{1}{S}\tau_{xy}$$
$$\gamma_{xz} = \frac{1}{S}\tau_{xz} \tag{2.7}$$
$$\gamma_{yz} = \frac{1}{S}\tau_{yz}$$

Where E is the Young's modulus, υ is Poisson's ratio, and S is the shear modulus. Fracture mechanics mostly deals with two-dimensional problems, in which the stresses and body forces are independent of one of the coordinates, here taken as z. Two-dimensional problems are of two classes. The first is plane stress problems in which the stresses in the z direction are zero as seen in Equation 2.8.

$$\sigma_{zz} = \tau_{zx} = \tau_{zy} = 0 \tag{2.8}$$

The second is plane strain problems where thickness is large. In this case, the strains towards z direction are small enough that they can be assumed to be zero.

$$\varepsilon_{zz} = \varepsilon_{zx} = \varepsilon_{zy} = 0 \tag{2.9}$$

For the infinitesimal body which is under the plane stress or strain condition, the equilibrium condition is expressed as follows:

$$\sum F_x = 0 \tag{2.10}$$
$$\sum F_x = \left(\sigma_{xx} + \frac{\partial \sigma_{xx}}{\partial x}dx\right)dydz + \left(\sigma_{xy} + \frac{\partial \sigma_{xy}}{\partial y}dy\right)dxdz - \sigma_{xx}dydz - \sigma_{xy}dxdz = 0$$

$$\frac{\partial \sigma_{xx}}{\partial x} dxdydz + \frac{\partial \sigma_{xy}}{\partial y} dydxdz = 0 \tag{2.11}$$

$$\frac{\partial \sigma_{xx}}{\partial x} + \frac{\partial \sigma_{xy}}{\partial y} = 0 \tag{2.12}$$

Similarly, for force components towards y direction, a similar expression can be deducted:

$$\sum Fy = 0 \longrightarrow \frac{\partial \sigma_{xy}}{\partial x} + \frac{\partial \sigma_{yy}}{\partial y} = 0 \tag{2.13}$$

when the two-dimensional case is taken in to consideration. Shear strain in the *x*-*y* plane are expressed in terms of the displacements *u* and *v*, respectively:

$$\gamma_{xy} = \frac{\partial u}{\partial y} + \frac{\partial v}{\partial x} \tag{2.14}$$

As the three strain components cannot be independent, an extra relation must exist between them. This relation is the compatibility equation of strain, and is obtained by eliminating u and v through differentiation of Equations 2.3 and 2.14.

$$\frac{\partial^2 \gamma_{xy}}{\partial y \partial x} = \frac{\partial^2}{\partial y^2}\left(\frac{\partial u}{\partial x}\right) + \frac{\partial^2}{\partial x^2}\left(\frac{\partial v}{\partial y}\right) \tag{2.15}$$

$$\frac{\partial^2 \gamma_{xy}}{\partial y \partial x} = \frac{\partial^2 \varepsilon_{xx}}{\partial y^2} + \frac{\partial^2 \varepsilon_{yy}}{\partial x^2} \tag{2.16}$$

Since; $\varepsilon_{xy} = \frac{\gamma_{xy}}{2}$;

$$2\frac{\partial^2 \varepsilon_{xy}}{\partial y \partial x} = \frac{\partial^2 \varepsilon_{xx}}{\partial y^2} + \frac{\partial^2 \varepsilon_{yy}}{\partial x^2} \tag{2.17}$$

For plane elasticity problems, the stress field ahead of a crack tip problem must satisfy all equilibrium requirements. As a particular technique is used in differential equations, the aim is to construct a general function that satisfies the partial differential equations. The same technique is used in the solution of the stress field ahead of the crack problems, except for the general function which is called Airy's Stress Function. According to Airy's stress function, equations can be described as:

$$\sigma_{xx} = \frac{\partial^2 \Phi}{\partial y^2} \tag{2.18a}$$

$$\sigma_{yy} = \frac{\partial^2 \Phi}{\partial x^2} \tag{2.18b}$$

$$\sigma_{xy} = \frac{\partial^2 \Phi}{\partial x \partial y} \tag{2.18c}$$

where Φ qualifies as an Airy stress function, it must fulfill the biharmonic equation. Because strain components can be written as the functions of stresses, Equation 2.17 can be formed by the combination of stress function in Equation 2.18 as follows:

$$\frac{\partial^4 \Phi}{\partial y^4} + 2\frac{\partial^4 \Phi}{\partial y^2 \partial x^2} + \frac{\partial^4 \Phi}{\partial x^4} = 0 \quad or \quad \nabla^4 \Phi = 0 \tag{2.19}$$

Two different complex variable methods have been used into the formulation of the two-dimensional elasticity problems: the first approach was introduced by Goursat-Kolosov and then it was modified by Muskhelishvili. Despite the fact that this approach has been widely used to solve singular problems, it is mathematically very demanding. However, another complex-variable method which is used only for straight crack problems, offers mathematical simplicity. This approach was introduced in 1939 by Westergaard. Originally, this method could be applied only to infinite body problems under remote stress condition (Shah et al., 1995). The method was modified in 1966 by Sih and again in 1972 by Eftis and Liebowitz (Eftis, 1972). To accommodate unequal remote biaxial loads, the method still had restricted applications. Fortunately, the Goursat-Kolosov representation of the Airy stress-

function for planar crack problems was connected with Westergaard notation. The new method is now suitable for all infinite and finite body problems with arbitrary boundary conditions.

The principle behind this is that all analytic functions are potential Airy stress functions. A function is analytic and Airy stresses function only if it satisfies the following condition:

$$\frac{\partial \operatorname{Re} Z}{\partial y} = -\frac{\partial \operatorname{Im} Z}{\partial x} = -\operatorname{Im} Z' \tag{2.20a}$$

$$\frac{\partial \operatorname{Im} Z}{\partial y} = -\frac{\partial \operatorname{Re} Z}{\partial x} = \operatorname{Re} Z' \tag{2.20b}$$

The equations are also known as Cauchy-Riemann relations. The prime superscript symbolizes differentiation with respect to the complex variable z. According to these relationships, the real and imaginary parts of Airy stress-functions can be separated independently. Consider an Airy stress function of the form:

$$\Phi(z) = \operatorname{Re} \tilde{\tilde{Z}}(z) + y\left(\operatorname{Im} \tilde{Z}(z) + \operatorname{Im} \tilde{Y}(z)\right) \tag{2.21}$$

where;

$$\begin{aligned} \frac{d\tilde{\tilde{Z}}}{dz} &= \tilde{Z} \\ \frac{d\tilde{Z}}{dz} &= Z \\ \frac{d\tilde{Y}}{dz} &= Y \end{aligned} \tag{2.22}$$

The Airy stress function from equation 2.21 can be used to solve the Cartesian stress components which are obtained from an Airy stress function through the second derivatives in respect to the real variables x, and y (Equation 2.19) via Cauchy-Riemann relations.

$$\sigma_{xx} = \frac{\partial^2 \Phi}{\partial y^2} = \mathrm{Re}\, Z - y\left(\mathrm{Im}\, Z' + \mathrm{Im}\, Y'\right) + 2\,\mathrm{Re}\, Y \tag{2.23a}$$

$$\sigma_{yy} = \frac{\partial^2 \Phi}{\partial x^2} = \mathrm{Re}\, Z - y\left(\mathrm{Im}\, Z' + \mathrm{Im}\, Y'\right) \tag{2.23b}$$

$$\sigma_{xy} = \frac{\partial^2 \Phi}{\partial x \partial y} = -\mathrm{Im}\, Y - y\left(\mathrm{Re}\, Z' + \mathrm{Re}\, Y'\right) \tag{2.23c}$$

Westergaard chose the complex functions *Z(z)* and *Y(z)*, and examined the central crack problem in his paper as follows:

$$Z(z) = \frac{\sigma z}{\sqrt{z^2 - a^2}} \tag{2.24a}$$

$$Y(z) = 0 \tag{2.24b}$$

$$Z'(z) = \frac{\sigma a^2}{\sqrt{\left(z^2 - a^2\right)^3}} \tag{2.24c}$$

Z(z) is analytic at all points in the *x*-*y* plane, except $z=\pm a$. Where "*a"* is half the length of crack in infinite plate, *z* is a complex function where $z=x+iy$ According to the chosen functions, cartesian stress components can be written as:

$$\sigma_{xx} = \frac{\partial^2 \Phi}{\partial y^2} = \mathrm{Re}\, Z - y\left(\mathrm{Im}\, Z'\right)$$

(2.25a)

$$\sigma_{yy} = \frac{\partial^2 \Phi}{\partial x^2} = \mathrm{Re}\, Z - y\left(\mathrm{Im}\, Z'\right) \tag{2.25b}$$

$$\sigma_{xy} = \frac{\partial^2 \Phi}{\partial x \partial y} = -y\left(\mathrm{Re}\, Z'\right) \tag{2.25c}$$

Figure 2.4 represents the multiple coordinate systems. Thus, auxiliary polar coordinates can be defined by the relations according to Equation 2.26:

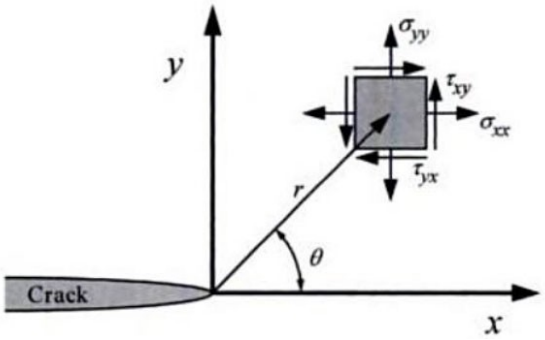

Figure 2.4 Definition of the coordinate axis ahead of a crack tip. The z direction is normal to the page (Anderson, 2005).

$$z-a=(x-a)+iy=r_1e^{i\theta_1} \tag{2.26a}$$

$$z+a=(x+a)+iy=r_2e^{i\theta_2} \tag{2.26b}$$

Thus, the stress components can be illustrated by the relations below:

$$\sigma_{xx}=\frac{\sigma r}{\sqrt{r_1r_2}}\cos\left(\theta+\frac{\theta_1+\theta_2}{2}\right)-\frac{\sigma a^2}{(r_1r_2)^{\frac{3}{2}}}r_1\sin\theta_1\sin\frac{3}{2}(\theta_1+\theta_2) \tag{2.27a}$$

$$\sigma_{yy}=\frac{\sigma r}{\sqrt{r_1r_2}}\cos\left(\theta+\frac{\theta_1+\theta_2}{2}\right)+\frac{\sigma a^2}{(r_1r_2)^{\frac{3}{2}}}r_1\sin\theta_1\sin\frac{3}{2}(\theta_1+\theta_2) \tag{2.27b}$$

$$\sigma_{xx}=\frac{\sigma a^2}{(r_1r_2)^{\frac{3}{2}}}r_1\sin\theta_1\sin\frac{3}{2}(\theta_1+\theta_2) \tag{2.27c}$$

The unknowns r, r_2, θ, θ_2 can be considered zero. Thus stress components near the crack tip can be written as functions with variables a, r_1, and θ_1.

$$\sigma_{xx}=\frac{\sigma\sqrt{\pi a}}{\sqrt{2\pi r_1}}\cos\frac{\theta_1}{2}\left[1-\sin\frac{\theta_1}{2}\sin\frac{3\theta_1}{2}\right] \tag{2.28a}$$

$$\sigma_{yy}=\frac{\sigma\sqrt{\pi a}}{\sqrt{2\pi r_1}}\cos\frac{\theta_1}{2}\left[1+\sin\frac{\theta_1}{2}\sin\frac{3\theta_1}{2}\right] \tag{2.28b}$$

$$\sigma_{xy} = \frac{\sigma\sqrt{\pi a}}{\sqrt{2\pi r_1}} \cos\frac{\theta_1}{2} \sin\frac{\theta_1}{2} \cos\frac{3\theta_1}{2} \tag{2.28c}$$

Since there is a stress singular zone around the crack tip in which state of stress is adequately represented by a single parameter, K (the stress intensity factor SIF), gives the strength of the singular field for small values of r_1. Thus, when this stress state becomes critical, a small crack grows and the material fails. This critical value is called fracture toughness in some sources since it is a criterion for material strength. The Mode-I *SIF*, K_I, can be expressed as follows:

$$K_I = \lim_{r\to 0} \sqrt{2\pi r}\,\sigma_{yy}(x, 0) \tag{2.29}$$

Applying this definition to the σ_{yy} stress for the central-crack problems from Equation 2.28b, it can be found that;

$$K_I = \sigma\sqrt{\pi a} \tag{2.30}$$

This is the *SIF* for mode-I type of loading for infinite sheet with a central-crack. However, this formulation can be modified for various geometries by an additional geometry function. It measures the strength of the singular field at the crack tip.

2.2.2 Energy Analysis Approach

As briefly described in the history of Fracture Mechanics, Griffith introduced the energy approach for crack propagation in glass in 1915. It was later generalized by Irwin who collected all available data to crack extension into a single term G_c, called the strain energy release rate. Although the term rate generally refers to a derivative with respect to time, here it does not. The term G_c is the rate of change in potential energy with crack area. According to crack propagation in size, sufficient potential

energy must be available to overcome the surface energy of the material. The Griffith Energy Theory for an increase in the crack area *d*a, can be expressed as:

$$\frac{dE_T}{da} = \frac{d\Pi}{da} + \frac{dW_S}{da} = 0 \tag{2.31}$$

In Equation 2.31, E_T describes the total energy, Π is the potential energy supplied by internal strain energy and external force, and W_S presents work required for creating a new surface. There, the derivative of potential energy with respect to incremental area of crack equals to the derivative of potential energy with respect to incremental area of crack according to the theorem of minimum potential energy;

$$\frac{d\Pi}{da} = -\frac{dW_s}{da} \tag{2.32}$$

To show that W_S is the change in the elastic surface energy due to formation of the crack surface, consider an infinite plate of unit thickness that contains a crack length *2a* subjected to uniform tensile stress, σ, as shown in Figure 2.5. W_S can be expressed as follows:

$$W_S = 4a\gamma_S \tag{2.33}$$

where γ_S is the surface energy of material. According to Inglis (Shah, 1995) , the change in the strain, *Π*, can be written as;

$$\Pi = -\frac{\pi\sigma^2 a^2}{E} \tag{2.34}$$

Thus;

$$\frac{dW_s}{da} = 4\gamma_S \tag{2.35a}$$

$$\frac{d\Pi}{da} = -\frac{2\pi\sigma^2 a}{E} \tag{2.35b}$$

Therefore, Equation 2.32 can be rewritten as:

$$2\gamma_S = \frac{\pi\sigma^2 a}{E} \tag{2.36}$$

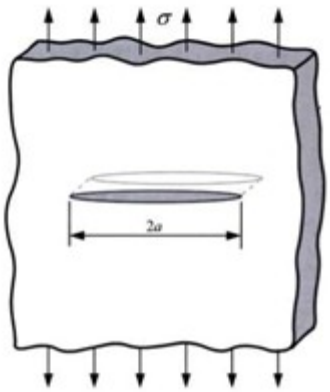

Figure 2.5 Infinite plate with crack subjected to tension

Therefore, for plane stress:

$$\sigma_c = \sqrt{\frac{2\gamma_s E}{\pi a}} \tag{2.37a}$$

For plane strain;

$$\sigma_c = \sqrt{\frac{2\gamma_s E}{\left(1-\upsilon^2\right)\pi a}} \tag{2.37b}$$

Later in 1957 (Shah, 1995), Irwin collected all sources of resistance to crack extension into a single term G_c energy release rate. Accordingly, the Irwin form of energy criterion can be written as:

For plane stress;

$$\sigma_c = \sqrt{\frac{EG_c}{\pi a}} \tag{2.38a}$$

For plane strain;

$$\sigma_c = \sqrt{\frac{EG_c}{\left(1-\upsilon^2\right)\pi a}} \tag{2.38b}$$

where G_c is the strain energy release rate. The energy analysis approach proposes a more convenient way for solving engineering problems.

2.2.3 Relationship between Stress Intensity Factor & Energy Release Rate

Since both the stress intensity factor and the strain energy release rate are criteria which present a bulk material property, a relationship between K and G must exist. Fortunately, these two material properties were developed as the extension of the Griffith condition and applied only to the same geometry used, in an infinite sheet under remote tension with a crack 2a long, as shown in Figure 2.5. Therefore, from the theory developed in the previous chapter, at the instant of instability, the following is obtained:

$$K_c = \sigma\sqrt{\pi a} \tag{2.39}$$

Comparing Equations 2.37a and 2.38 for the same failure events in LEFM case reveals that;

For plane stress;

$$K_c^2 = EG_c \tag{2.40a}$$

For plane strain;

$$K_c^2 = \frac{EG_c}{1-\upsilon^2} \tag{2.40b}$$

Although this generalization seems valid for an infinite sheet under remote tension, this relationship between *G* and *K* for any geometry or crack configuration is admissible for LEFM.

2.3 General Principles of Nonlinear Elastic Fracture Mechanics (NLEFM) Approach

As introduced previously, energy principles can be used to describe critical energy for crack propagation for nonlinear elastic, elastic-plastic and quasi-brittle material properties. In the linear case, when the energy reaches a critical value, catastrophic failure occurs. However, in nonlinear materials, a crack may steadily propagate up to a critical length. NLEFM concept can be evaluated by using three main approaches as follows;

- Fracture Resistance Curve (R-Curve)
- J-integral method
- Crack Tip Opening Displacement

Fracture Resistance Curve can be used to characterize energy release rate to create a unit crack area in the domain. Generally, it is a function of structural geometry and material fracture properties. LEFM allows the stress to approach infinity at crack tip. Since infinite stress cannot develop in real materials, a certain range of inelastic zone must exist at the crack tip. This inelastic zone around a crack tip is termed fracture

process zone (FPZ). If the fracture process zone is small enough to ignore, function may be regarded to depend only on the material geometry. Briefly, a structure with an initial crack a_0 and unit thickness should be considered. U is the total strain energy produced by a load P. In this case, the energy release rate is a function of the crack length a and the applied load P. It can be formulated as follows:

$$G_q = \left[\frac{\partial U}{\partial a}\right]_P \tag{2.41}$$

Here G_q is a strain energy release rate in the nonlinear case. The crack propagation at the crack tip requires consuming energy W. Therefore, the fracture resistance R can be expressed as a function of crack extension as well as energy release rate. The second-order derivative of potential energy can be considered to obtain sufficient condition to identify the stability of crack propagation as follows;

$$\frac{\partial \Pi}{\partial a} = R - G_q \tag{2.42}$$

$$\frac{\partial^2 \Pi}{\partial a^2} = \frac{\partial R}{\partial a} - \frac{\partial G_q}{\partial a} \tag{2.43}$$

Taking all these into account, several important observations can be made about unstable fracture. The critical SIF is no longer a material property. As such, the critical SIF depends on the geometry and the fracture process zone. Figure 2.6 shows three different loads P_1, P_2 and P_3 where $P_3>P_2>P_1$. Although the curves corresponding to P_1 and P_2 reach the critical point of the resistance curve, the crack propagates even though the load decreases. Therefore, the relationship between R-curve and the strain energy release rate can be archived as;

- For stable crack growth $\longrightarrow$ $\frac{\partial R}{\partial a} - \frac{\partial G_q}{\partial a} > 0$
- For stationary crack growth $\longrightarrow$ $\frac{\partial R}{\partial a} - \frac{\partial G_q}{\partial a} = 0$
- For unstable crack growth $\longrightarrow$ $\frac{\partial R}{\partial a} - \frac{\partial G_q}{\partial a} < 0$

Unstable crack growth generally ends with catastrophic failure. In the case of stable crack growth, the crack can have an extension at the point of fracture toughness of material and this phenomenon continues until it gets to an unstable crack growth.

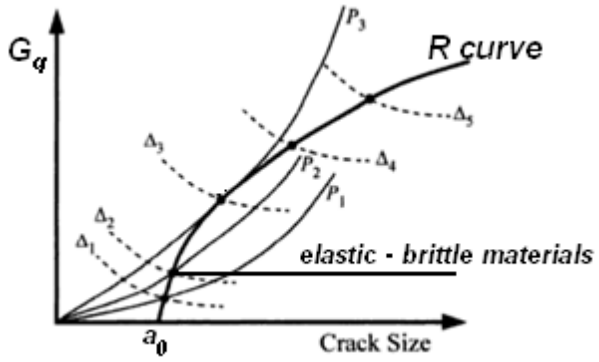

Figure 2.6 Schematic view of R-curve (Anderson, 2005).

Later, Rice proposed a new assumption to evaluate the energy release rate in nonlinear elastic materials, which is known as the J-Integral method (Rice, 1968):

$$J = \int_{\Gamma} \left[U_d \left(a, \in\right) d_y - T \frac{\partial u}{\partial x} d_s \right] \tag{2.44}$$

Where "Γ" is a counterclockwise closed contour path surrounding the crack tip. U_d is the density of strain energy, $T=(T_x,T_y)$ is the tension vector perpendicular to Γ in the outside direction and $u=(u_x,u_y)$ is the displacement vector at ds as shown below:

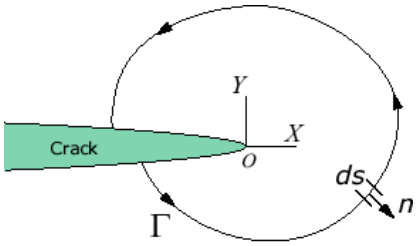

Figure 2.7 J-Integral contour.

It should be noted that for elastic-plastic and quasi-brittle materials the value obtained by J-integral is path-dependent. Additionally, it is valid only if the fracture process zone is relatively small as regards the size of the region within the contour *Γ*. Only when the inelastic zone is within the contour path, J-Integral method partially account for the influence at the crack tip. Otherwise, the strain energy release rate cannot be predicted.

Wells introduced that the crack tip opening distance may be described as the fracture criterion of inelastic materials (Wells, 1961). He worked on the same infinite plate with the crack size 2*a* (Figure 2.5) to evaluate the crack opening distance criteria crack opening the distance (COD) and the crack tip opening distance (CTOD) as referred to in Figure 2.8:

$$COD = \frac{4\sigma}{E}\sqrt{a^2 - x^2} \tag{2.45}$$

By introducing the inelastic zone r_p, Equation 2.45 becomes;

$$COD = \frac{4\sigma}{E}\sqrt{\left(a + r_p\right)^2 - x^2} \tag{2.46}$$

Since CTOD is the position of COD where *x* is equal to the crack length *a* as follows;

$$CTOD = \frac{4\sigma}{E}\sqrt{2ar_p} \tag{2.47}$$

According to Irwin (Irwin, 1960), the fracture process zone can be calculated by using the yield strength

$$r_p = \frac{K_I}{2\pi\sigma_{ys}^2} \tag{2.48}$$

By combining of equations 2.48 and 2.46, CTOD can be written as:

$$CTOD = \frac{4\sqrt{2}K_I^2}{E\pi\sigma_{ys}} \tag{2.49}$$

Equation 2.49 is only valid for linear elastic materials. However, this phenomenon is modified for concrete and quasi-brittle materials. The following chapter presents nonlinear approaches for concrete found in literature. Additionally, it points out the how crack opening distance can be used as critical fracture a criterion in concrete.

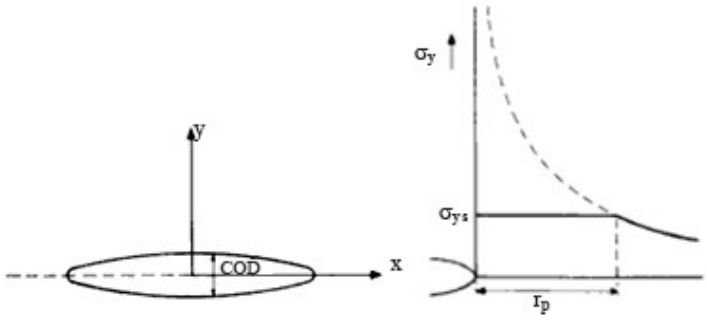

a-) Crack opening distance b-) Plastic zone at the crack tip

Figure 2.8 Plastic zone in inelastic materials.

2.4 Fracture Mechanics of Concrete

2.4.1 Fictitious Crack Approach

Fracture behavior of concrete is mainly influenced by the fracture process zone as that zone is quite large in comparison to crack size. In Figure 2.9, a crack model for concrete is presented where an initial crack with length a_0 and associated fracture process zone Δa are described. In that figure, the concrete is assumed to have quasi-brittle behavior. The cohesive pressure $\sigma(w)$ is a monotonic decreasing function of crack separation displacement w. This model does not include the micro cracks ahead of the crack tip. For the concrete fracture model, the energy release rate is prejudiced by two different portions (Bažant, 2002),

1. The energy release rate consumed by creating two surfaces, $G_{Ic.}$
2. The energy rate to overcome the cohesive pressure, $\sigma(w)$, in separating the surfaces $G_{\sigma.}$

Thus the energy release rate for a Mode-I quasi-brittle crack, G_q can be expressed as;

$$G_q = G_{Ic} + G_\sigma \tag{2.50}$$

The value of G_{Ic} can be calculated by using LEFM and it is called critical energy release rate. Since G_q is equal to the work done by cohesive pressure with unit thickness, the expression may be evaluated as follows;

$$G_\sigma = \frac{1}{\Delta a}\int_0^{\Delta a}\int_0^{w}\sigma(w)dxdw = \frac{1}{\Delta a}\int_0^{\Delta a}dx\int_0^{w}\sigma(w)dw = \int_0^{w_t}\sigma(w)dw \tag{2.51}$$

where w_t represents crack separation displacement at the initial crack tip. w_c is the critical crack separation. If crack separation is large enough, w_t can be higher than w_c.

In other words, cohesive pressure function may be equal to zero at the tip of the real crack as shown in Figure 2.9. In this case w_t should replace w_c.

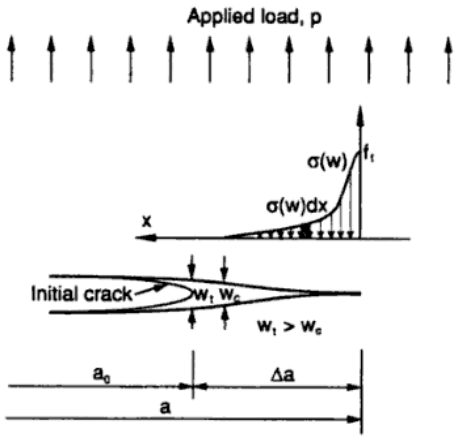

Figure 2.9 A cohesive crack with partially separated crack surface (Shah, 1995).

Fictitious crack model for concrete was first proposed by Hillerborg (Hillerborg, 1976). The general idea behind the fictitious crack approach is that the energy to create a new surface is rather small compared to the energy required to separate them. Thus the energy release rate term, G_{Ic}, vanishes. Regarding this, Hillerborg used a concrete plate subjected to uniaxial tension as shown in Figure 2.10. As shown in Figure 2.10, two different gages were used to measure the displacements for elongation including the cracked section and outside the crack section respectively. After reaching a peak load, gage A and gage B have independent and different stress – elongation curves. Since the energy release rate is assumed to be vanished, the stress – elongation curve according to gage A after the post peak fracture behavior is denoted as G_F, as shown in the Figure 2.10, which is given by;

$$G_F = \int_0^{w_c} \sigma(w)dw \tag{2.52}$$

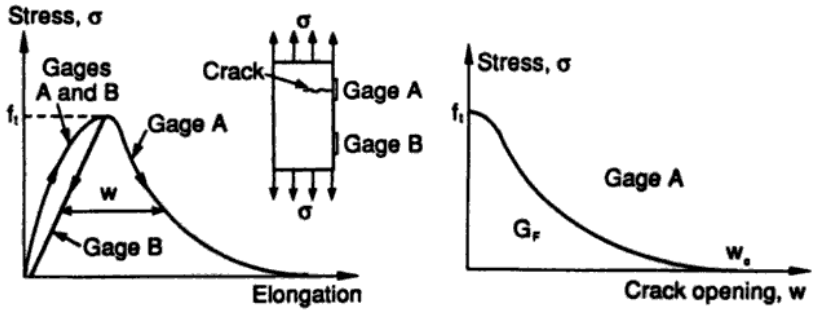

Figure 2.10 Complete tensile stress-elongation curve for fictitious crack model by Hillerborg (Shah, 1995).

In his model, Hillerborg assumed that the stress – separation function, $\sigma(w)$, has an independent characteristic of structure, geometry, and size. Therefore this model requires one to know three parameters for concrete which are f_t, G_F, and the shape of stress separation curve, $\sigma(w)$.Where f_t is the tensile strength of concrete. According to this information, he introduced a parameter which is known as characteristic length;

$$l_f = \frac{EG_F}{f_t} \tag{2.53}$$

The value of characteristic length for concrete generally ranges from 1 cm to 4 cm (Shah et al., 1995). l_f is proportional to the length of fracture process zone based on the fictitious crack model, and it is purely a material property.

Another effective fictitious concrete fracture model was proposed by Bažant and Oh (Bažant et al., 1983). They modeled the fracture process zone as an imaginary band of uniformly and continuously distributed micro cracks with a fixed width, h_c. Then, they used a simple stress strain model for the crack's quasi-brittle behavior as shown in Figure 2.11.

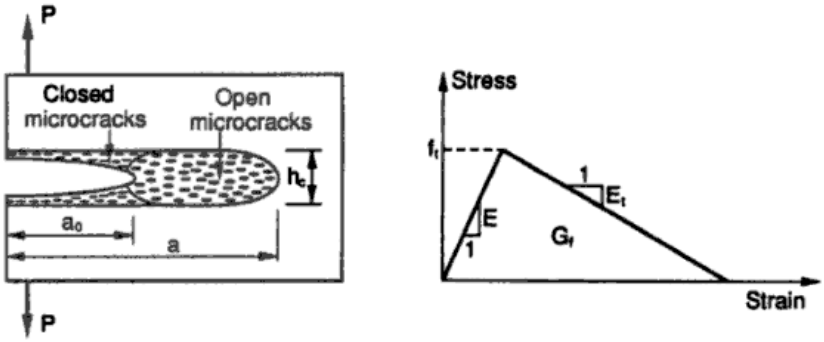

Figure 2.11 A micro crack band model and stress strain curve for crack band model (Shah, 1995).

According to Equation 2.54, Bažant and Oh proposed the energy consumption by crack propagation for unit area of crack band, G_f, which is the area under the stress-strain curve;

$$G_f = h_c\left(1+\frac{E}{E_t}\right)\frac{f_t^2}{2E} \tag{2.54}$$

where E is modulus of elasticity, E_t presents the strain softening modulus, f_t is the tensile strength of concrete, and h_c is an empirical bandwidth number. h_c is an approximate function which can be calculated as;

$$h_c = d_a n_a \tag{2.55}$$

where n_a is an empirical constant which is generally 3 for concrete and d_a is the maximum aggregate size (Bažant et al., 1983).

2.4.2 Effective-Elastic Crack Approach

Contrary to fictitious crack models, in effective - elastic crack models, concrete fracture criterion is modeled by an assumption that the stress - separation function, $\sigma(w)$, is neglected. Therefore, fracture process zone effect must be included in the calculation. Hence, this model is governed by LEFM behavior. As a result, the energy release rate for Mode-I type loading may be calculated as;

$$G_q = G_{Ic} \tag{2.56}$$

where G_q is a function of structural size and applied load as well as crack length and orientation. Since the crack length will increase by increment of the loading for the case of stable crack propagation, an additional equation should be provided to calculate the effective crack length. Unfortunately, since this effective crack length depends on geometry and size, it may not be used as an independent and unique fracture criterion. Thus, another fracture quantity should be introduced. Therefore, the general approach of effective-elastic crack approach uses more than one criterion.

Jenq and Shah's approach which is known as the "Two parameter fracture model" can be introduced as one of the most popular concrete effective elastic fracture models (Jenq and Shah, 1985). In their two-parameter fracture model, in order to separate the elastic and plastic responses of a given specimen, Jenq and Shah loaded the specimen up to a maximum stress and then they unloaded and reloaded it as shown in Figure 2.12.

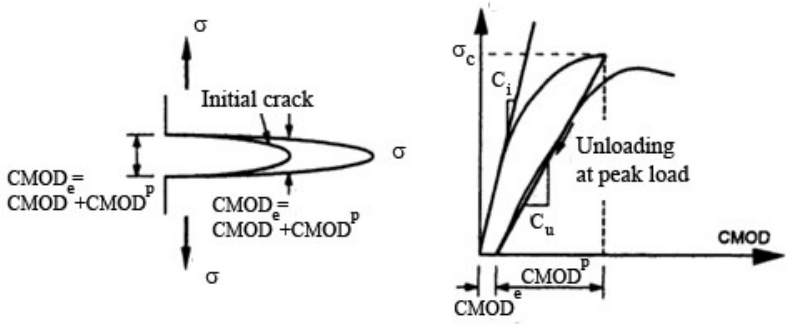

Figure 2.12 Elastic and plastic fracture responses and loading and unloading procedure (Jenq and Shah, 1985).

As it is seen above, crack mouth opening distance, $CMOD_c$, is separated into two parts, elastic ($CMOD_c^e$) and plastic ($CMOD_c^p$). Basic LEFM formulations to calculate the critical stress intensity factor, or fracture toughness, K_{Ic}, and the critical effective elastic crack length, a_c, are valid for their model after $CMOD_c$, and σ_c are measured. According to LEFM laws, K_{Ic}, $CTOD_c$ and $CMOD_c$ may be calculated as;

$$K_{Ic} = \sigma_c \sqrt{\pi a_c}\, g_1\left(\frac{a_c}{b}\right) \tag{2.57}$$

$$CMOD_c^e = \frac{4\sigma_c a_c}{E}\, g_2\left(\frac{a_c}{b}\right) \tag{2.58}$$

$$CTOD_c^e = CMOD_c^e\, g_3\left(\frac{a_c}{b}, \frac{a_o}{a_c}\right) \tag{2.59}$$

According to experimental results obtained from three-point bending test, Jenq and Shah found that beams with different sizes but made of the same material have identical K_{Ic}, $CMOD_c$, g_1, g_2, and g_3. Here g_1, g_2, and g_3 are geometrical functions Since in the two-parameter fracture model, the crack exhibits a compliance equal to the unloading compliance, the model determines the critical fracture state of a structure based on its elastic response. Although the two-parameter model has been accepted, calibration of model requires stiff machines which can unload when 95

percent of ultimate load is reached followed by reloading. They also introduced a parameter which is known as a material length, Q, expressed as follows;

$$Q = \left(\frac{E \cdot CMOD_c}{K_{Ic}} \right)^2 \tag{2.60}$$

Higher values of Q mean a more ductile material. According to their experimental observations, they proposed that K_{Ic}, $CTOD$, and E can be calculated by using the compressive strength of concrete, f_c as follows;

$$K_{Ic} = 0.06\left(f_c\right)^{0.75} \tag{2.61}$$

$$CTOD_c = 0.00602\left(f_c\right)^{0.13} \tag{2.62}$$

$$E = 4785\sqrt{f_c} \tag{2.63}$$

where K_{Ic} is in $MPa\sqrt{m}$ and $CTOD_c$ is millimeters, and E and f_c are in MPa. Another reason to use the two parameter model to the predict fracture process of concrete is that all materials in nature have flaws, and when concrete is loaded, these flaws may propagate and directly be linked with the crack tip. Although in ductile materials, a single parameter can be used to predict fracture toughness, brittle materials, especially concrete, require more than one parameter because of the size of the wake process zone. Therefore, $CTOD_c$ is used together with K_{Ic} to determine the critical crack propagation for quasi-brittle materials.

In 1990, Bažant and Kazemi introduced a simulation of fracture of quasi-brittle materials by a modified version of Bažant and Ohs' crack band model by means of effective-elastic crack approach (Bažant and Kazemi, 1990). They used a series of three-point bending test specimens with the constant ratio of initial crack length (a_o) to the dimension of depth (D). For these geometrically similar structures with a_o, they found that the nominal stress failure may be described as follows:

$$\sigma_c = \frac{c_n P_c}{tD} \tag{2.64}$$

where P_c is the peak load, t is the thickness of specimen, D represents the depth, and S is the span for a three-point bending test specimen as shown in Figure 2.13;

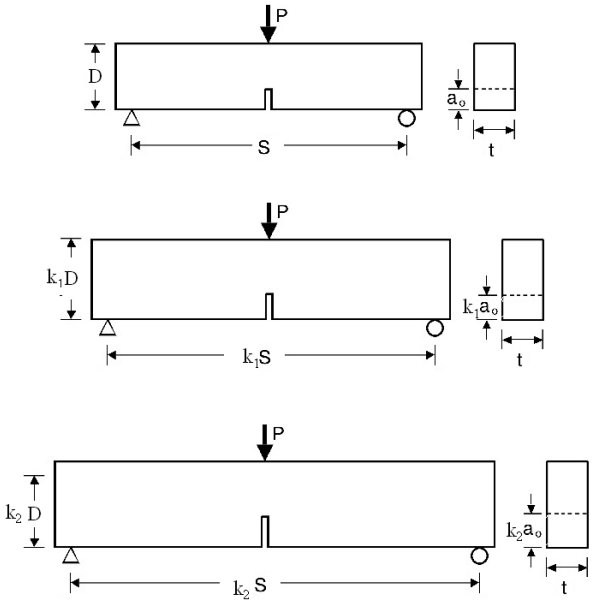

Figure 2.13 Series of geometrically similar three-point bending test structures.

c_n is a constant which can be calculated in linear case as follows ;

$$c_n = \frac{1.5S}{D} \tag{2.65}$$

Bažant and Kazemi used the expression above for LEFM formulations. According to their model, the critical energy release rate for a certain size of concrete structure can be written as:

$$G_{Ic} = \frac{K_{Ic}^{\ 2}}{E} = \frac{\sigma_c^{\ 2}\pi a_c}{E} g_1^{\ 2}\left(\frac{a_c}{D}\right) = \frac{P_c^2}{Et^2 D} g\left(\frac{a_c}{D}\right) \tag{2.66}$$

where again $a_c = a_o + \Delta a$ is the critical crack length and $g\left(\frac{a_c}{D}\right)$ is a geometric function which is given by;

$$g\left(\frac{a_c}{D}\right) = \frac{c_n{}^2 \pi a_c}{D} g_1{}^2\left(\frac{a_c}{D}\right) \tag{2.67}$$

Bažant, in his previous studies, worked on the failure stress of the geometrically similar structures. He, then, demonstrated that up to $\frac{D}{D_o} = \frac{1}{20}$ nominal stresses can be expressed as follows:

$$\sigma_{Nc} = \frac{Bf_t}{\sqrt{1 + \frac{D}{D_o}}} \tag{2.68}$$

where B is a constant based on the effective elastic crack approach and D_o is another constant which is called characteristic size. Bažant and Kazemi proposed using a critical energy release rate and critical crack extension for an infinitely large structure in order to eliminate the length of the crack extension. Therefore, two different parameters are defined in their article;

$$G_f = \lim_{D\to\infty} G_{Ic} = \lim_{D\to\infty} \frac{\sigma_{Nc}{}^2 \pi D}{Ec_n{}^2} g\left(\frac{a_c}{D}\right) = \frac{B^2 f_t{}^2 \pi D_o}{Ec_n{}^2} g\left(\frac{a_o}{D}\right) \tag{2.69}$$

As discussed previously, another parameter is necessary to obtain a fracture mechanism of concrete. The authors introduced the second parameter as critical crack extension, c_f, for an infinite large specimen. In order to obtain the critical crack extension, they expanded the geometric function $g\left(\frac{a_f}{D}\right)$ into a Taylor series only up to first order terms as follows;

$$c_f = \lim_{D\to\infty} \Delta a_c \tag{2.70}$$

$$g\left(\frac{a_f}{D}\right) \approx g\left(\frac{a_o}{D}\right) + g'\left(\frac{a_o}{D}\right)\left(\frac{a_f}{D} - \frac{a_o}{D}\right) = g\left(\frac{a_o}{D}\right) + g\left(\frac{a_o}{D}\right)'\left(\frac{c_f}{D}\right) \tag{2.71}$$

where;

$$a_f = a_o + c_f \tag{2.72}$$

As a result, the critical crack extension for large specimen can be expressed as;

$$c_f = \frac{g\left(\frac{a_o}{D}\right)}{g'\left(\frac{a_o}{D}\right)} D_o \tag{2.73}$$

In 1991, Planas and Elices compared the fictitious crack model, the size effect model, and the two parameter fracture model. For that purpose, a series of similar three-point bending beam structures were tested. The values of G_f, G_{Ic}^s were obtained from the size effect model and the two-parameter model for comparisons. As a result of those experiments, they obtained $G_f = 0.52\ G_F$ and $G_{Ic}^s = 0.48\ G_F$ as D approaches infinity. Therefore G_f and G_{Ic}^s are comparable. It is also noted that G_{Ic}^s or G_f is the rate of strain energy required to extend a crack. On the other hand, G_F is the energy per unit area to completely to separate a fracturing material. Therefore, the value of G_F is approximately twice as great as the values of G_f and G_{Ic}^s. It is also reported that the peak load prediction for an infinitely large structure by the size effect model and the two parameter fracture model are 28.1 and 30.8 % lower than the one predicted by the fictitious crack model (Planas and Elices, 1992).

2.5 Finite Element Analysis of Fracture Mechanics Properties

2.5.1 Finite Element Modeling of Singularities

In finite element modeling of cracks and stress singular parts of structure, it is necessary to have not only very refined mesh but also special elements at the crack tip. Three main approaches are developed to improve the accuracy of FEM and to obtain more realistic solutions:

i. Enriched finite elements
ii. Singular finite elements
iii. Hp-finite elements

In general, in finite element analysis, finer meshes usually yield solutions that are closer to the exact solution. However, it is not always the case for the fracture mechanics analysis. As mentioned in the previous sections, there is an inverse square root singularity at the crack tip. Singular finite elements are the most popular solutions to solve this kind of singularities. For one layered domain, Barsom in 1976 demonstrated that mathematical exact solution of square root singularity can be obtained by replacing the mid-side nodes to the quarter point position. The concept of the quarter-point singular element was generalized by Staab in 1983. Therefore, by varying the placement of the mid-side node, it is possible to model any singularity.

In order to understand the concept of quarter point singular elements, the formulation of shape function of isoparametric singular finite elements can be explained for one-dimensional elements as shown in Figure 2.14. The equation is given as follows:

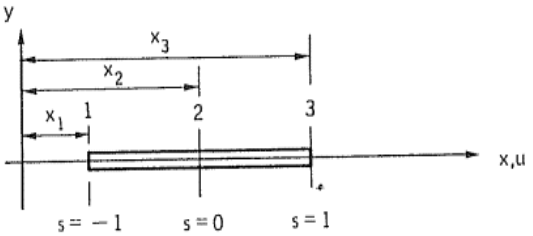

Figure 2.14 Three-node bar element (Carpinteri et al., 2007).

$$u = \sum_{i=1}^{3} N_i u_i \tag{2.74}$$

$$x = \sum_{i=1}^{3} N_i x_i \tag{2.75}$$

$$x = \sum_{i=1}^{3} N_i x_i = N_1 x_1 + N_2 x_2 + N_3 x_3 \tag{2.76}$$

Here u is the displacement function and N_i is the shape function in which the displacement is equal to 1 at the i^{th} point. For 3 nodes 1-D elements, geometry functions are shown in Figure 2.15;

In order to replace the mid-node, the nodes can be defined as follows;

$$\begin{aligned} x_1 &= 0 \\ x_2 &= wl \\ x_3 &= l \end{aligned} \tag{2.77}$$

"*l"* is the length of the element. A variable "*w*" can be used to make mid-node variable. Thus, the displacement function "*x*" might be written as below;

$$x = \left(1 - s^2\right) wl + \left(\frac{1+s}{2} - \frac{1-s^2}{2} \right) l$$

$$\frac{x}{l} = \left(w + \frac{s}{2} + \frac{1-2w}{2} \right) \tag{2.78}$$

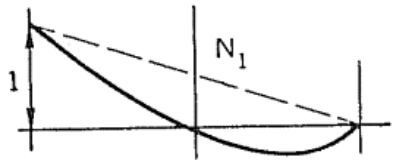

$$N_1 = \frac{1}{2}(1-s) - \frac{1}{2}(1-s^2)$$

a) N_1.

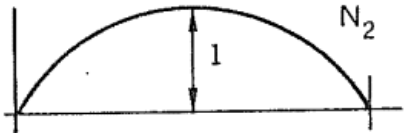

$$N_2 = 1-s^2$$

b) N_2.

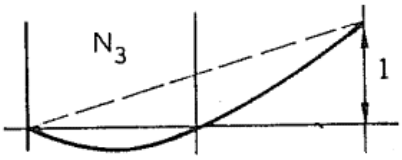

$$N_3 = \frac{1}{2}(1-s) - \frac{1}{2}(1-s^2)$$

c) N_3.

Figure 2.15 Linear interpolation shape functions for 3-node bar elements (Carpinteri et al., 2007).

The parameter "*w*" controls the order of stress-singularity. For instance, obtaining a quarter-point finite element, we should set *w=1/4* for crack stress singularity in one layered (homogenous) materials. Thus, the following expression for "*s*" is obtained:

$$s = -1 + 2\sqrt{\frac{x}{l}} \tag{2.79}$$

Consequently, the displacement function can be expressed as follows;

$$u = \sum_{i=1}^{3} N_i u_i = \left[1 - 3\sqrt{\frac{x}{l}} + 2\left(\frac{x}{l}\right)\right]u_1 + \left[4\sqrt{\frac{x}{l}} - 4\left(\frac{x}{l}\right)\right]u_2 + \left[-\sqrt{\frac{x}{l}} + 2\left(\frac{x}{l}\right)\right]u_3 \quad (2.80)$$

As a result, the stress components along x-coordinate tend to go to infinity as x goes to 0, with a power of singularity equal to negative square root;

$$\lim_{x\to 0}\varepsilon_x = \lim_{x\to 0}\frac{\partial u}{\partial x} \propto \lim_{x\to 0}\frac{1}{\sqrt{x}} \to \infty \quad (2.81)$$

$$\lim_{x\to 0}\sigma_x = \lim_{x\to 0}E\varepsilon_x = \lim_{x\to 0}E\frac{\partial u}{\partial x} \propto \lim_{x\to 0}\frac{1}{\sqrt{x}} \to \infty \quad (2.82)$$

Since stress goes to infinity at the crack tip, FEM model and the exact mathematical model of domain can have a better match. Therefore, the calculation of stress singularity at the crack tip is able to have more realistic results according to mesh size and stress singular elements at the crack tip. In the FE computer package ANSYS©, there is a special meshing tool which defines a concentration key point about which area mesh will be skewed. During skewing, a user can specify the position of the key point at the midpoint or quarter point as shown in Figure 2.16.

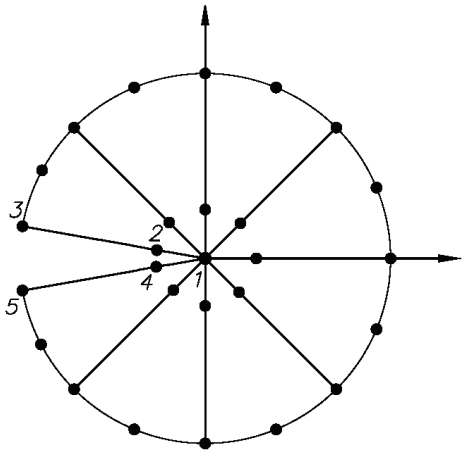

Figure 2.16 Singular elements at the crack tip and nodes used in calculation of SIFs.

It is recommended that for the best accuracy, length of each singular element at the crack tip should be less than eight times of crack length, and angle at the crack tip should be between 30^o and 40^o (Cook et al., 2001)

2.5.2 Calculation of Stress Intensity Factor Using Finite Element Method

In the previous sections, it is mentioned that SIF is calculated to obtain the stress singularity value at the crack tip for different modes of crack. As aforementioned, in this study the problem of a crack in a concrete under LEFM condition is presented. In FEM, there are three main methods presented in the literature to estimate SIF as follows (ACI, 2009);

- Displacement Correlation Technique (DCT)
- Stress Correlation Technique (SCT)
- Energy release rate methods
    - J-Integral Method
    - Potential energy derivative approaches

In this study, to obtain force "P" versus mid span displacement "δ" curve of a beam in bending crack propagation analysis is performed by DCT. Moreover, to see effect of meshing and elements types, DCT results are compared with handbook calculations.

The displacement correlation technique has been a widely used technique to evaluate the stress intensity factor since FEM and computer applications became an important part of analyses. Kim and Paulino evaluated Mode-I and mixed-mode two-dimensional problems (Kim and Paulino, 2002). In this thesis, displacement correlation technique is utilized by application of linear elastic fracture mechanics for concrete. In brief, a three-dimensional crack front under Mode-I loading as shown in Figure 2.19 is considered (ACI, 2009).

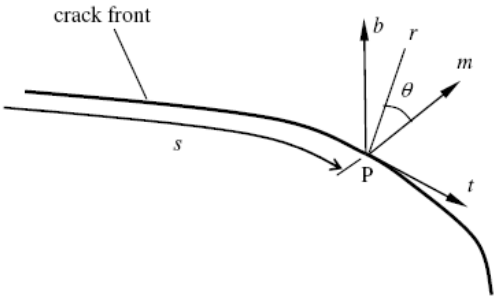

Figure 2.17 Crack Front and the Local Coordinate System.

The parameter "*s*" in Figure 2.19 is the arc length of the crack front. "*b", "m", "t"* represent axes of the local coordinate system located at point "*P*". The parameters *"r"* and *"θ"* are the polar coordinates in the normal plane (*m, b*). The asymptotic distribution of the normal stress and displacement components at point *P* can be expressed as follows;

$$\sigma_{bb}(r,\theta)=\frac{K_I(s)}{\sqrt{2\pi r}}\cos\left(\frac{\theta}{2}\right)\left[1+\sin\left(\frac{\theta}{2}\right)\sin\left(\frac{3\theta}{2}\right)\right] \tag{2.83}$$

$$u_{bb}(r,\theta)=\frac{1+\nu^P}{E^P}\sqrt{\frac{2r}{\pi}}K_I(s)\sin\left(\frac{\theta}{2}\right)\left[2\left(1-\nu^P\right)-\sin^2\left(\frac{\theta}{2}\right)\right] \tag{2.84}$$

Figure 2.21 shows deformed crack surface and 2 nodes after crack propagation.

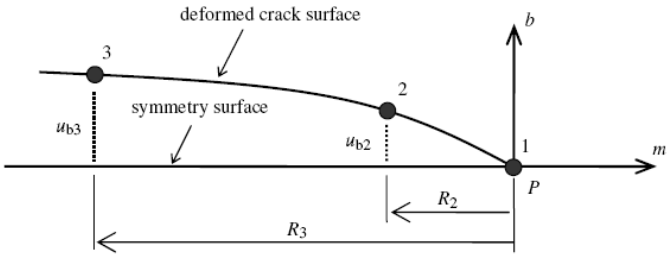

Figure 2.18 Deformed Crack Surface.

Using equation 2.84, the displacement field on the crack surface (u_{bb}) can be written as;

$$u_b(r,\pi) = \frac{4\left(1+v^{P^2}\right)}{E^P}\sqrt{\frac{r}{2\pi}}K_I \tag{2.85}$$

The stress intensity factor for mode I can be expressed as follows;

$$K_I = \frac{E^P\sqrt{2\pi}}{4\left(1+v^{P^2}\right)}\lim_{r\to 0}\left(\frac{u_b(r,\pi)}{\sqrt{r}}\right) \tag{2.86}$$

While "*r*" goes to zero, an undefined case near the crack tip occurs. The linear extrapolation technique can be used to evaluate the equation;

$$\frac{u_b(r,\pi)}{\sqrt{r}} \cong Ar + B \tag{2.87}$$

The expressions for two different boundary conditions can be formulated as follows;

When $r=R_2$, $u_b=u_{b2}$
When $r=R_1$, $u_b=u_{b1}$

Therefore, for case 1;

$$\frac{u_b(R_2,\pi)}{\sqrt{R_2}} = \frac{u_{b2}}{\sqrt{R_2}} = AR_2 + B \tag{2.88}$$

For case 2;

$$\frac{u_b(R_1,\pi)}{\sqrt{R_1}} = \frac{u_{b1}}{\sqrt{R_1}} = AR_1 + B \tag{2.89}$$

Using Equations 2.88 and 2.89, new equations can be evaluated as unknowns "*A"*, and "*B"*;

$$A = \frac{\sqrt{R_2}u_{b3} - \sqrt{R_3}u_{b2}}{\sqrt{R_2}\sqrt{R_3}(R_3 - R_2)} \tag{2.90}$$

$$B = \frac{R_3^{3/2}u_{b3} - R_2^{3/2}u_{b2}}{\sqrt{R_2}\sqrt{R_3}(R_3 - R_2)} \tag{2.91}$$

If "*r"* value is very small, "*A"* value vanishes at the crack tip. Therefore, the expression $\frac{u_b(r,\pi)}{\sqrt{r}}$ will be equal to "*B"* as "*r"* equals to zero.

$$K_I = \frac{E^P\sqrt{2\pi}}{4\left(1+v^{P^2}\right)}B \tag{2.92}$$

Using equations 2.91 and 2.92, the stress intensity factor K_I can now be expressed as below.

$$K_I = \frac{E^P\sqrt{2\pi}}{4\left(1+v^{P^2}\right)}\frac{R_3^{3/2}u_{b3} - R_2^{3/2}u_{b2}}{\sqrt{R_2}\sqrt{R_3}(R_3 - R_2)} \tag{2.93}$$

As presented above, after the finite element calculation, by using displacements and distances at crack tip of the two nodes on the crack surface, it is easy to find SIF.

2.5.3 The Main Feature and Hypothesis of Finite Element Analysis of Fracture in Concrete

It became apparent that concrete structures usually do not behave in a way consistent with the assumption of classical continuum mechanics (Bažant, 1976). Fortunately, in the work done so far, it has been mentioned that two approaches may be used to estimate concrete fracture behavior by FEM.

The first approach is known as the smeared crack model. The smeared crack approach was first introduced by Rashid. This approach is based on the concept of replacing a crack by a continuous medium with altered properties (Rashid, 1968). The earliest approach is to change the element stiffness to zero, once the stress is calculated to exceed the tensile strength capacity of the material. Over the years, numerical applications of smeared crack model have been challenged by the strain localization problem.

The second approach, discrete crack model is an elder, however still widely used finite element model to evaluate crack propagation and fracture damage of structure for concrete and quasi-brittle materials. There are three problems to be solved: determining the location and initiation direction of the initial crack, determining how the crack extends, and determining the direction of crack extension. The first issue can be solved on the basis of maximum tensile stress. Crack extension may be determined for LEFM problems by considering the SIF associated with stress state at the crack tip. When SIF exceeds the fracture toughness, the crack propagates. Alternatively, energy release rate can be used. After this process, the crack length should be increased, then remeshing will be performed to incorporate the new crack direction and the same process must be executed up to structure failure occurs or the model cannot take any more load. Remeshing is the main disadvantage of the discrete crack model.

Nowadays, the cohesive crack model is widely used for the analysis of propagating cracks in concrete and other quasi brittle materials. In Figure 2.19, a schematic description of crack propagation for concrete is presented. Two different zones can be distinguished in this figure. The left is the stress free zone, where crack faces are completely stress-free. The faces are completely disconnected. The Second zone on the right is the damage zone also called the fracture process zone. As it can be seen in Figure 2.19, there are micro cracks and flaws in this zone. This case is totally different from LEFM. However, as explained earlier, there are some ways to convert the LEFM approach into the cohesive approach.

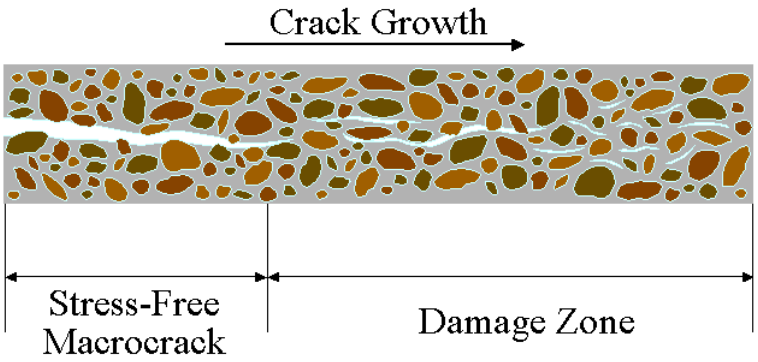

Figure 2.19 Cohesive crack model and damage zone in concrete (Carpinteri et al., 2007).

From 1984 to 1989 Carpinteri tried to figure out how Hillerborg's fictitious model can be used for finite element analysis. He proposed that nonlinear behavior of concrete at the damage zone can be subjected to the nodes after increasing crack length as shown in the figure below;

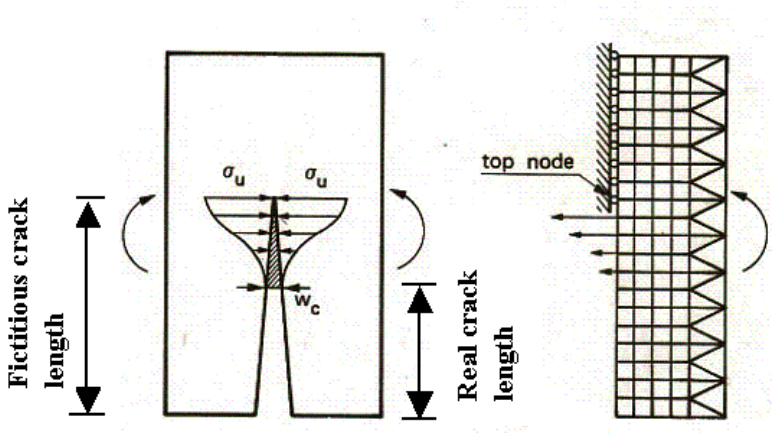

Figure 2.20 Finite element view of discrete crack model (Carpinteri et al., 2007).

In finite element calculation, formulation of cohesive traction forces can be calculated as follows;

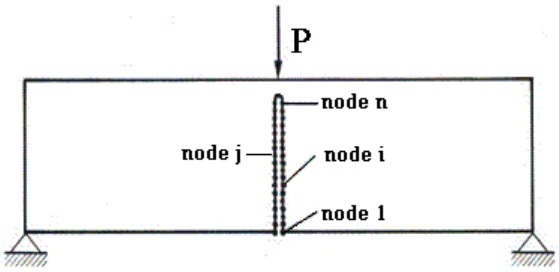

Figure 2.21 Finite element analysis of three-point bending beam (Carpinteri et al., 2007).

If the damage zone is absent;

$$\{w\} = [K]\{F\} + \{C\}P \tag{2.94}$$

where, w is the vector of the crack opening distance, [K] is the matrix of the coefficients of influence when subjected to force of a unit. {F} is vector of the nodal cohesive traction force; {C} is vector of the coefficients of influence when domain is subjected to the force P.

If the damage zone is present between nodes j and n, cohesive forces can be calculated as follows;

$$\begin{Bmatrix} F_i = 0 & for\ i = 1,.....,(j-1) \\ F = F_t\sigma(w) & for\ i = j\ ,.....,n \\ w_i = 0 & for\ i > n \end{Bmatrix} \tag{2.95}$$

Consequently, cohesive traction force in the quasi-brittle material is integrated into the model as shown in the fictitious crack model. In this case, concrete fracture criteria may be crack tip stresses. When it is equal to ultimate tensile stress of the material, crack propagation occurs. Discrete crack model laws are valid for this model, therefore, the crack length increases until the failure of model is observed.

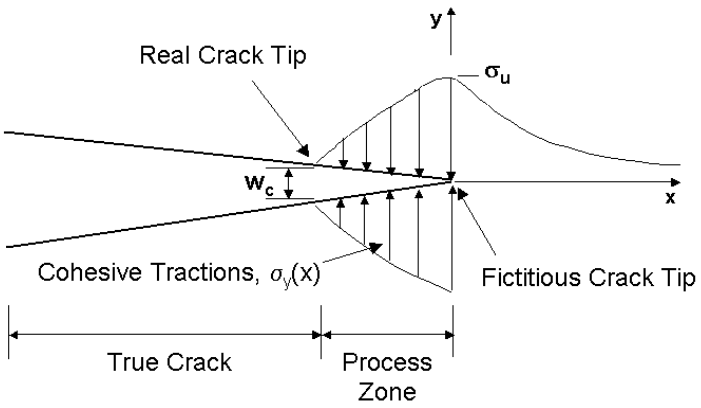

Figure 2.22 General review of stress distribution in fictitious crack model (Carpinteri et al., 2007).

In 2002 Bažant defined the limitation of the cohesive crack model as follows (Bažant, 2002);

- The crack model is a strictly uniaxial model. This seems just fine for standard notched specimens but is questionable for general application to a structure subjected to triaxial stresses.
- A very tortuous crack with adjacent zone of micro cracking and frictional slips is replaced by an ideal straight line crack, which introduces some error.
- The reason for a finite width "*h*" of energy dissipation zone probably is not so much the energy dissipated by micro cracking on the side of final crack path but mainly the energy dissipated by frictional slips by reinforcement, which represents at least 50% and perhaps 80% of G_f as shown in Figure 2.23

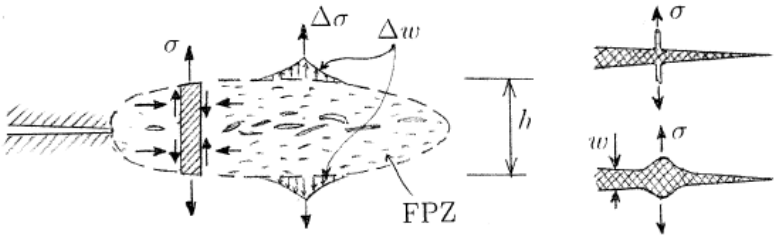

Figure 2.23 Triaxial stresses in the FPZ and its nonlocal behavior in reinforced concrete (Bažant, 2002).

As noted before, another way is to predict the SIF, then to consider the behavior of the material as LEFM, and increase the crack length according to a model chosen. Approach to be used may be fictitious or an effective elastic crack approach. However, the model should not assume ideally linear elastic behavior. Otherwise, the predicted fracture behavior can be miscalculated. Meshing must be paid special attention for crack problems, because of the high stress concentrations near the crack tip.

CHAPTER 3

INTRINSIC PARAMETERS OF FINITE ELEMENT ANALYSIS OF FRACTURE

In this chapter, the first objective of the thesis is investigated. For this purpose, earlier studies for finite element size in the finite element solutions of fracture of concrete are mentioned. Then the three-point bending test specimen in ASTM standards is compared with solution by FEM with various mesh sizes and element types. Thus, the accuracy of the finite element solutions is presented.

3.1 The Issue of Stability of Crack Propagation

The role of finite element size in the concrete fracture analysis was first presented by Carpinteri (Carpinteri et al., 2007). According to the work carried out by him and his coworkers, the mesh refinement was taken into consideration with respect to brittleness number. The brittleness number is related to not only material but also the geometry and size of structure. The greater value of the brittleness number, the more is the brittle characterized of the structure. In this study, brittleness number (or Carpinteri number) is described as follows:

$$SE = \frac{G_f}{\sigma_u h} \tag{3.1}$$

With this purpose, they used the cohesive crack model with 3 different mesh refinements which have 20, 40 and 80 elements at the fracture face, respectively, as shown in Figure 3.1. Providing the relationship between mesh refinement and

brittleness number they analyzed ten beams having various brittleness numbers as shown in Table 3.1.

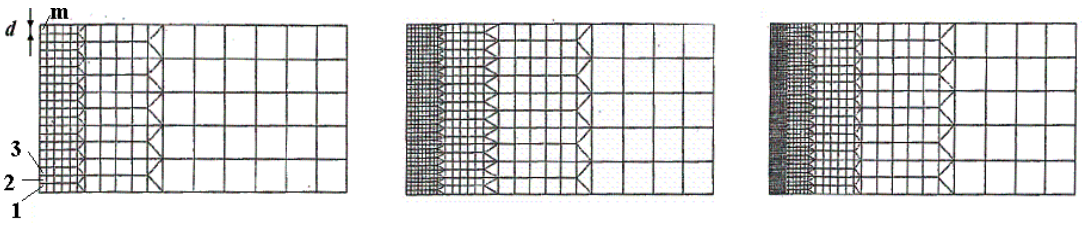

Figure 3.1 Mesh refinements with 20, 40, and 80 elements at fracture face (Carpinteri et al., 2007).

First, they used 20 elements at the fracture surface, then they have found some unexpected instable jumps and snap-back which are caused by the refinement of meshing as mentioned in Figure 3.2. Fortunately, they have figured out that increasing the mesh refinement can solve the instability problem as shown in Figure 3.2a and 3.2b. It can be seen in Figure 3.2c that snapback instabilities are eliminated by using 80 elements at the crack surface for all materials with a brittleness number higher than 0.21e-5

Table 3.1 The properties of beams analyzed by Carpinteri (Carpinteri et al., 2007).

Specimen Name	Brittleness Number($SE=G_f/\sigma_u h$)
L	2.09E-5
I	1.88E-5
H	1.67E -5
G	1.46E -5
F	1.25E-5
E	1.04E-5
D	0.84E-5
C	0.63E-5
B	0.42E-5
A	0.21E-5

Since the brittleness number (SE) can be related to the critical crack surface opening distance, the relationship between two can be presented as follows:

$$SE = \frac{G_f}{\sigma_u h} = \frac{w_c}{2h} = \frac{w_c}{2md} \tag{3.2}$$

where "*m"* is the number of elements at the path of crack propagation, "*d"* represents the size of the finite element. Consequently, Carpinteri and his coworkers assumed that, critical surface opening distance is equal to the 0.1 mm for ordinary concrete and a high brittleness number is 2.09E-5. Then, for their study they proposed that maximum size of the element should be calculated as follows:

$$\frac{w_c}{2md} \geq \frac{80e-5}{m} \Rightarrow d \leq 600 w_c \tag{3.3}$$

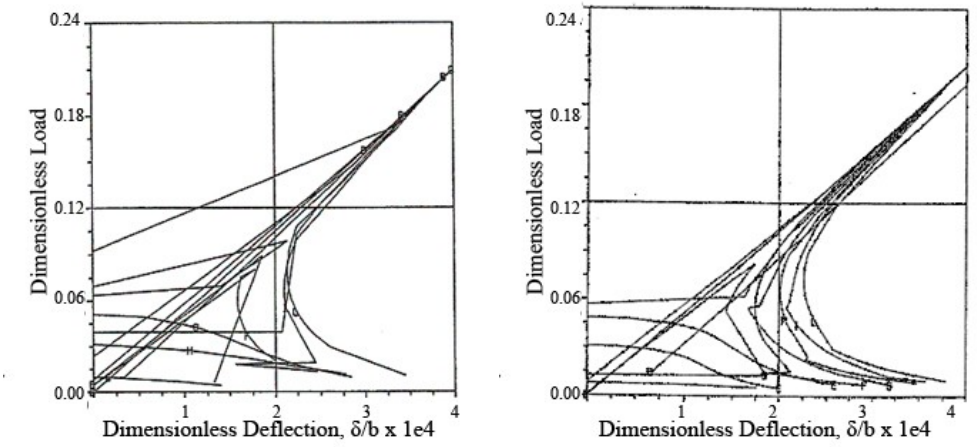

a) 20 elements at fracture process face b) 40 elements at fracture process face

Figure 3.2. Dimensionless load versus midpoint deflection curves for beams analyzed by Carpinteri (Carpinteri et al., 2007).

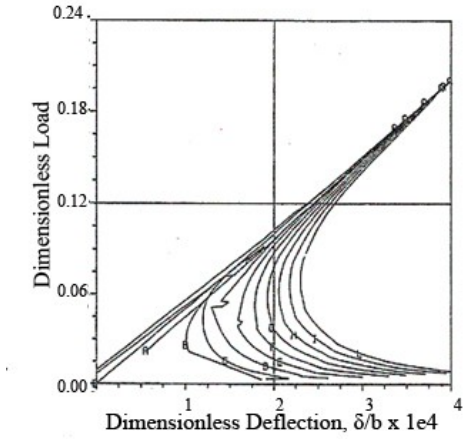

c) 80 elements at fracture process face

Figure 3.2. Dimensionless load versus midpoint deflection curves for beams analyzed by Carpinteri (Carpinteri et al., 2007). (Continued)

3.2 Finite Element Size and Types of Elements

The efficiency of the refinement of the mesh and quarter point elements have been pointed out previously. In order to check the accuracy of the finite element solution process and the element types, two different elements and three different mesh refinements have been executed in this thesis. During the analysis, ANSYS was used as a general purpose FE solver. The FE solver has special names for elements. In this section, the 8-node high order element which is called as “plane82” and the lower order 4-node “plane42” element are compared to emphasize the role of element types in fracture and failure analysis. Figure 3.3 and 3.4 show the elements’ shapes and interpolation points. It should be noted that 4-node elements do not have a mid-node that will be changed to quarter point of the element. Thus, the problem of singularity presented in section 2.5.1 will not be included to FEM.

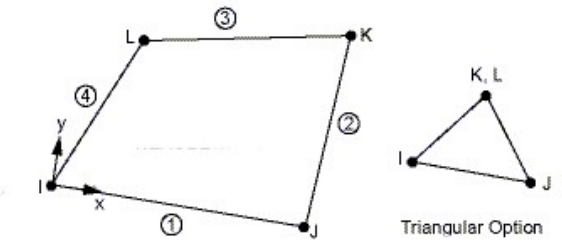

Figure 3.3 4-node “plane42” elements of ANSYS (ANSYS I. , 2004).

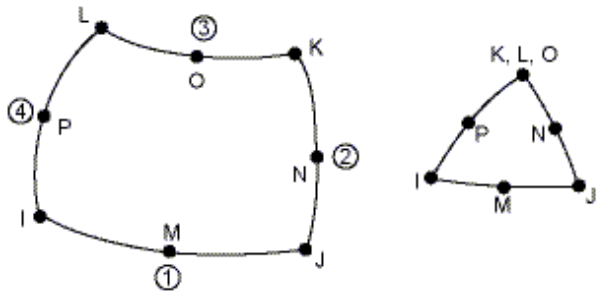

Figure 3.4 High order 8-node “plane82” elements of ANSYS (ANSYS I. , 2004)

The finite element analysis of fracture for different element types and sizes were compared to the analytical solution of beam specimens described in ASTM E-399.

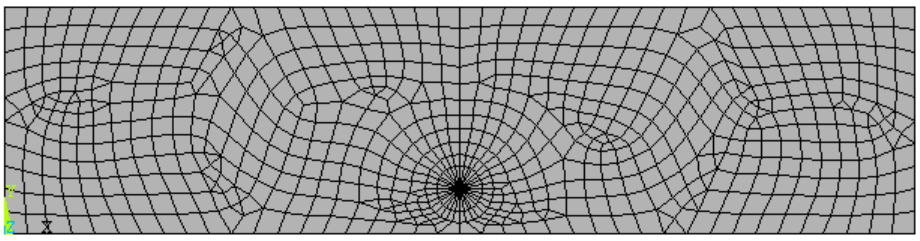

a) 13 elements at fracture surface.

Figure 3.5 Mesh resolutions of three-point bending specimen.

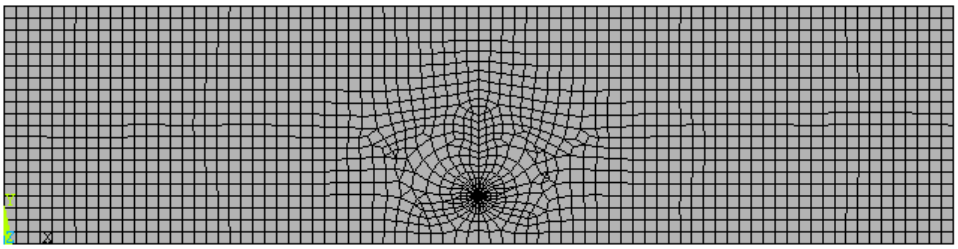

b) 23 elements at fracture surface.

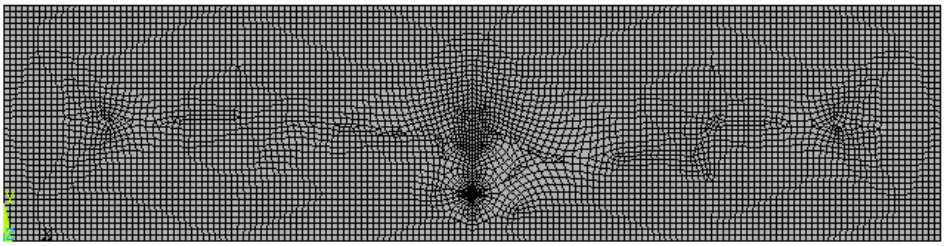

c) 43 elements at fracture surface.

Figure 3.6 Mesh resolutions of three-point bending specimen. (Continued)

In ASTM E-399, there are five specimen geometries certified for K_{IC} testing under the LEFM case (ASTM, 2005). The fracture resistance exhibits a thickness dependence on fracture resistance, due to the formation of a plastic zone around the crack tip (Sanforld, 2002) as shown in Figure 3.6. The material resistance to fracture behaves as a bulk material property after the point B_c, and its value can be accepted as a material criterion. However, LEFM solution can only be valid if ratio of length of fracture process zone, "r_p", on structure size, "D", is higher than 100 (Bažant Z. P., Concrete Fracture Models: testing and practice, 2002).

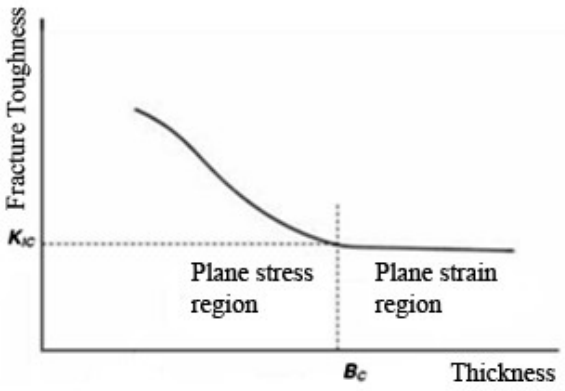

Figure 3.6 Relationship between SIF and thickness.

One of the most preferential test geometries for concrete is the bending specimen shown in Figure 3.7. It contains a single-edge notch with length "*a"*. "*W"* is the depth, and "*S"* is the span length. The test procedure requires a span to width ratio, *S/W* of 4. The standard bend specimen defined in Standard E 399 has a width-to–thickness ratio *W/B* equal to 2, but a range of values between 1 and 4 is permitted.

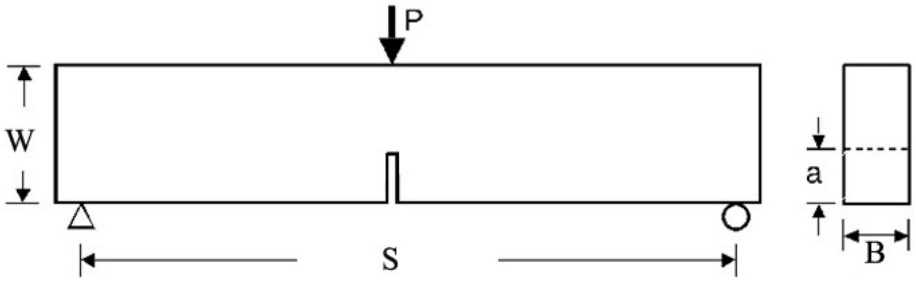

Figure 3.7 Three-point bending test procedure.

According to ASTM E-399, the provisional value of the material's SIF value when subjected to mid-point loading *P* of the specimen can be evaluated as follows;

$$K_I = \frac{PS}{BW^{\frac{3}{2}}} f\left(\frac{a}{W}\right) \tag{3.3}$$

Where $f\left(\frac{a}{W}\right)$ is the geometry function calculated by boundary collocation solutions and finite element modeling. When the fitting function is chosen carefully, it has been reported that results may have 0.5% error.

$$f\left(\frac{a}{W}\right)=\frac{3\left(\frac{a}{W}\right)^{\frac{1}{2}}\left[1.99-\left(\frac{a}{W}\right)\left(1-\frac{a}{W}\right)\left(2.15-3.93\frac{a}{W}+2.7\left(\frac{a}{W}\right)^{2}\right)\right]}{2\left(1+2\frac{a}{W}\right)\left(1-\frac{a}{W}\right)^{\frac{3}{2}}} \qquad (3.4)$$

As mentioned earlier, mesh refinement and efficiency of quarter point elements are studied for the beam specimen described in ASTM E 399. Accuracy and errors of the calculations related to the meshing can be seen in Table 3.2. As seen below, ratios of crack length on height of three-point bending test specimen are 0.2, 0.3, 0.4 0.5, 0.6, 0.7, and 0.8. All the meshes are provided in Appendix-A but in Figure 3.5 the meshing for an *a/w* ratio of 0.2 is provided. Table 3.2 presents the results obtained with 4-node elements;

Table 3.2 Impact of mesh size on SIF calculations with 4-node elements.

a/W	Number of Elements along the Crack	SIF Calculated by Ansys	SIF Calculated by ASTM	Error %
0.2	10	3.51	4.70	25.22
0.3		4.69	6.08	22.88
0.4		6.19	7.93	21.88
0.5		8.32	10.65	21.91
0.6		11.74	15.09	22.19
0.7		18.12	23.40	22.57
0.8		33.15	43.21	23.28
0.2	20	3.73	4.70	20.68
0.3		4.90	6.08	19.36
0.4		6.39	7.93	19.43
0.5		8.56	10.65	19.66
0.6		12.15	15.09	19.47
0.7		18.89	23.40	19.26
0.8		34.96	43.21	19.08
0.2	40	3.81	4.70	18.88
0.3		4.99	6.08	17.98
0.4		6.52	7.93	17.72
0.5		8.75	10.65	17.80
0.6		12.40	15.09	17.82
0.7		19.29	23.40	17.58
0.8		35.78	43.21	17.20

Table 3.2 shows that as the size of the element gets smaller the obtained SIF values become closer to the ASTM solutions. However, since the 4-node elements do not have a quarter-node, the results are not that accurate because of singularity as explained in section 2.5.1. Therefore, although error decreases with a finer mesh, results are still not in acceptance level, even for high number of elements. However, Table 3.3 presents the results obtained when high-order 8-node elements that have quarter-point nodes are utilized in the analysis. As predicted, the results, in Table 3.3,

are closer to mathematical model with a minor error for the 8-node high order elements with quarter point nodes.

Table 3.3 Impact of mesh size on SIF calculations with 8-node high-order elements.

a/W	Number of Elements along the Crack	SIF Calculated by		Error %
		Ansys	ASTM	
0.2		4.65	4.70	1.17
0.3		6.07	6.08	0.25
0.4		7.90	7.93	0.36
0.5	13	10.6	10.65	0.47
0.6		15.04	15.09	0.35
0.7		23.45	23.40	0.21
0.8		43.54	43.21	0.77
0.2		4.65	4.70	1.09
0.3		6.06	6.08	0.34
0.4		7.89	7.93	0.49
0.5	23	10.59	10.65	0.61
0.6		15.01	15.09	0.51
0.7		23.41	23.40	0.03
0.8		43.54	43.21	0.77
0.2		4.65	4.70	0.99
0.3		6.06	6.08	0.25
0.4		7.90	7.93	0.39
0.5	43	10.6	10.65	0.48
0.6		15.04	15.09	0.34
0.7		23.46	23.40	0.27
0.8		43.72	43.21	1.17

.

CHAPTER 4

CRACK PROPAGATION SIMULATION FOR STEEL FIBER REINFORCED CONCRETE

Steel fibers or fibers in general are utilized in concrete to control the tensile cracking and to increase its toughness. The effects of fiber geometry, fiber properties, fiber volume on the properties of fiber reinforced concrete are often experimentally studied (Banthia, 1994), (Oh, 2007). In this part of the thesis numerical simulation of a FRC beam under bending will be performed. The properties of the materials that are obtained from literature and the numerical simulation procedure will be explained in the proceeding sections.

4.1 Material Properties and Finite Element Types.

According to the experimental part of the work carried out by Oh in 2007, the compressive strength of plain concrete was 36 MPa and the flexural tensile strength was 4.8 MPa. The dimensions of the beam were 100 x 100 x 400 mm and the span length was 300 mm as shown in Figure 4.1. The load was applied in four-point loading condition in displacement control manner and the load versus mid-point deflection were determined. Specimens with fiber contents of 1% and 1.5% of the total concrete volume, respectively, were tested.

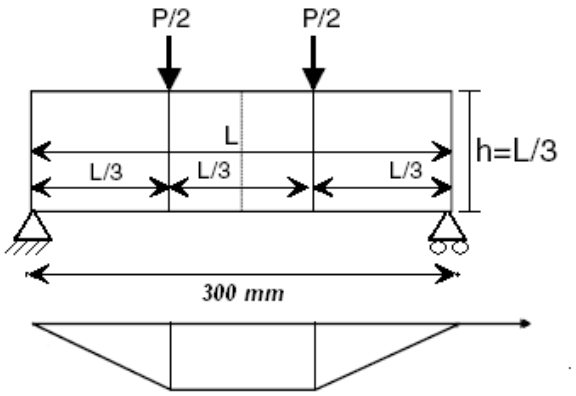

Figure 4.1 Experimental three-point bending test beam (Oh, 2007).

Due to the fact that there is not any experimental work to determine the fracture toughness of concrete in that experimental study, it is assumed that the tensile stress considering fictitious crack approach at the fracture process zone is an exponential function according to Gopalaratnam and Shah's model (Gopalaratman and Shah, 1985). The exponential function of cohesive forces on crack face is presented as follows;

$$\sigma(w) = f_t e^{-kw^{\lambda}} \tag{4.1}$$

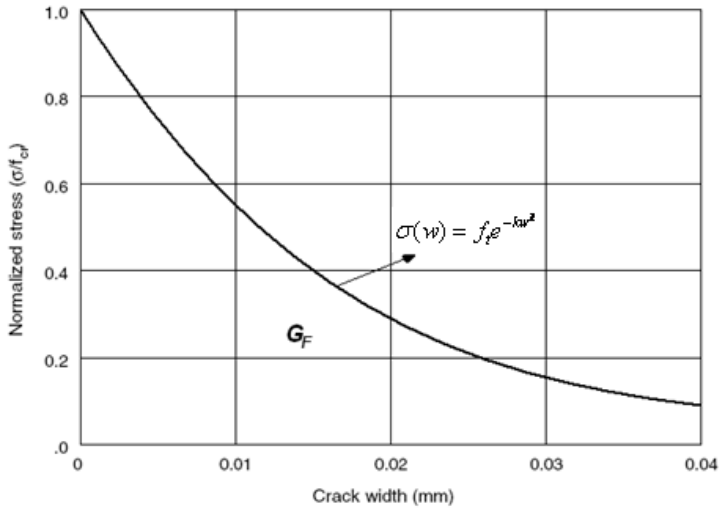

Figure 4.2 Gopalaratnam and Shah's strain softening model (Oh, 2007).

where $\sigma(w)$ is the tensile stress function (cohesive function), w presents crack opening displacements at node, k is an empirical constant and it is 60.8 in this case, λ is again an empirical constant that is equal to 1.01. Although the fracture propagation in the process of extension is assumed to be a linear phenomenon, the energy needed for crack propagation i.e. energy release rate, is assumed to be approximately equal to energy which is produced by cohesive forces as presented in the fictitious crack approach, G_F. As mentioned in Equation 2.29a, $G_F = (K_{IC})^2/E$. Therefore, the brittleness number can be calculated as follows:

$$S_E = \frac{G_f}{\sigma_u h} = \frac{\int_0^{w_c} f_t e^{-kw^\lambda} dw}{4.8 \cdot 100} = 1.71e-4 \tag{4.2}$$

From Equation 3.2, maximum element size can be calculated as follows;

$$\frac{w_c}{2md} > 1.71e-4 = d < 5.86mm \tag{4.3}$$

Thus, element size must be less than 5.86 mm for 20 elements at fracture surface. There are numerous studies and approaches in literature, which investigate pullout characteristics of steel fibers as a function of several variables, including the rate of loading, and steel fiber and concrete properties. In addition, a number of matrix and fiber modifications are examined to improve the bond-slip characteristics of fibers of various shapes (Oh B. H., 2007). In his 2006 work, Oh first proposed to determine the optimum shape of a structural synthetic fiber and then to explore experimentally and numerically the flexural behavior of steel fiber reinforced concrete beam. In that study, various types of fibers were subjected to pull out test as shown in Figure 4.3.

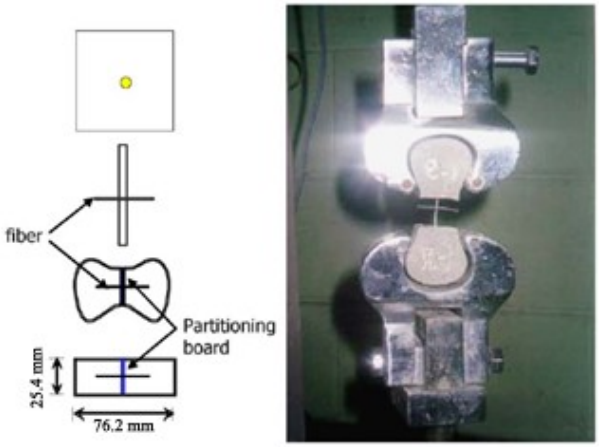

Figure 4.3 Pull out experiment of steel fibers (Oh, 2007).

After numerous tests of various types of fibers, the test results of energy capacities for various shapes of fibers are shown and the crimped-shape structural synthetic fibers were found to exhibit the highest energy absorption capacity. Therefore they proposed the average pullout test load versus slip relation obtained for this type of fiber. In Oh's study, it is suggested that the load–slip equation obtained from the tests is described as follows;

$$F_P = \frac{aS}{b + cS^d} \tag{4.2}$$

where F_P is pull-out force, S is the slip and a, b, c, d are constants to be obtained from Oh's test results. When value of slip exceeds 4.5 mm, F_P can be selected as 0.07 kN a shown in Figure 4.4;

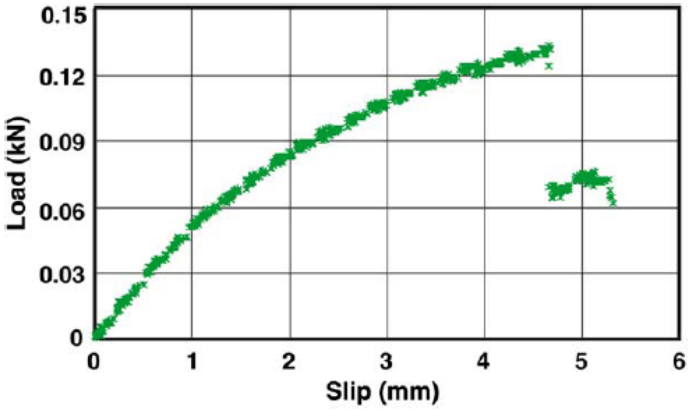

Figure 4.4 Slip-Load curve for crimped-shape steel fiber(Oh, 2007).

Using Oh's formulation for slip of the fiber from concrete matrix, the load deformation characteristics of a fiber reinforced concrete beam specimen was numerically investigated. In the numerical simulation study performed using ANSYS, fiber effect is included by unidirectional elements with nonlinear generalized force-deflection capability with element type COMBIN39. The element has longitudinal capability in 2-D, or 3-D applications. The longitudinal option is a uniaxial tension-compression element with up to three degrees of freedom at each node, translations in the nodal *x*, *y*, and *z* directions. No bending or torsion is considered for this element. In this thesis, uniaxial tension behavior of element is included as a function proposed by Oh presented in Equation 4.2.

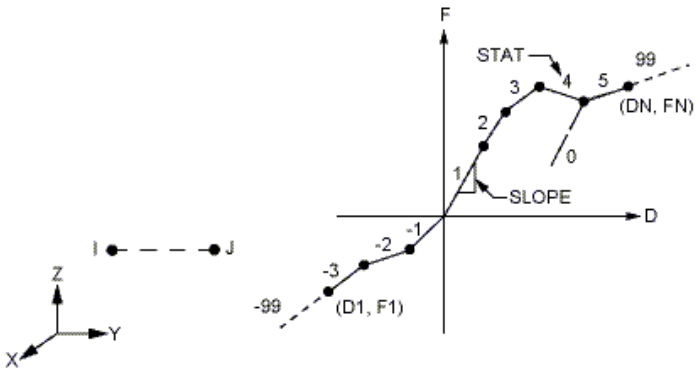

Figure 4.5 Behavior and inputs for COMBIN39 type of element (ANSYS I, 2004).

Since nonlinear elements have been selected to use in solution, nonlinearity may be included by using iterative series of linear solution. In ANSYS, the Newton-Rapson Method or Arc-Length method are used for the solution of nonlinear problems. Newton-Rapson method is selected to solve the nonlinearity problem.

4.2 Fiber Orientation Factor

P. Soroushian and Cha-Don Lee introduced a formulation for the number of fibers per unit cross-sectional area for various volume fractions of fibers (Soroushian and Cha-Don Lee, 1990). They proposed the number of fibers per unit area, N_1, as follows.

$$N_1 = \alpha \frac{V_f}{A_f} \tag{4.3}$$

where A_f presents the cross-sectional area of steel fibers, V_f is the volume fraction of steel fibers in the concrete, α is the orientation factor. In an infinitely large volume of concrete, fibers are expected to be randomly oriented with the same probabilities but in different directions in space. However, when parallel boundaries exist, the fibers located near boundaries are in a situation somewhere between three-dimensional and two-dimensional random orientations. The orientation factor α may be considered as the effective factor that an arbitrarily-oriented fiber is perpendicular to the crack plane. Therefore, in 1990, Soroushian and Lee presented a formulation to easily select an orientation factor for cases with four boundaries as presented in Figure 4.6.

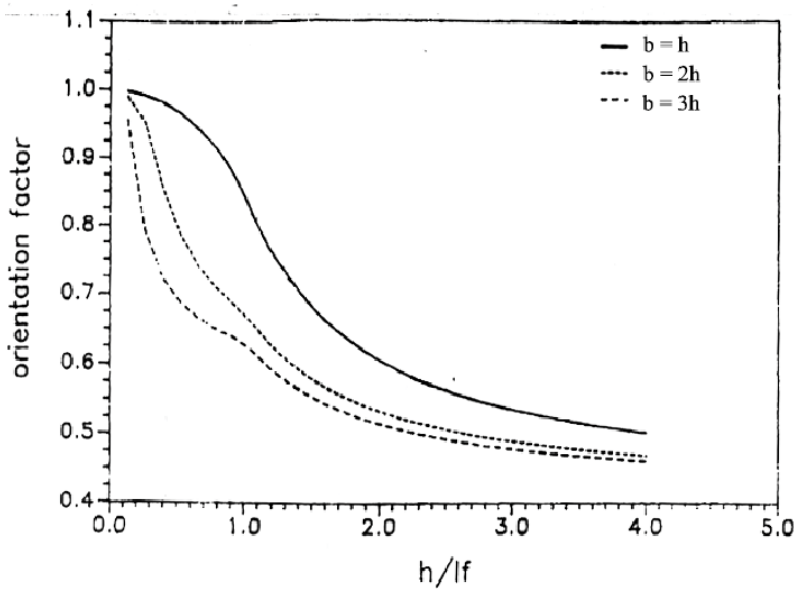

Figure 4.6 Orientation factor with various cross-sectional dimensions. (Soroushian, 1990)

Here *lf* is the length of the fiber, *h* is the height of the beam specimen. As pointed out earlier, when the height of the structure restrains, the orientation factor for a specified direction becomes larger. Therefore, Soroushian and Lee reported the orientation factor for a two-side restrained condition (Soroushian, 1990). Hence, they recommended using different conditions for four boundaries as shown in Figure 4.7.

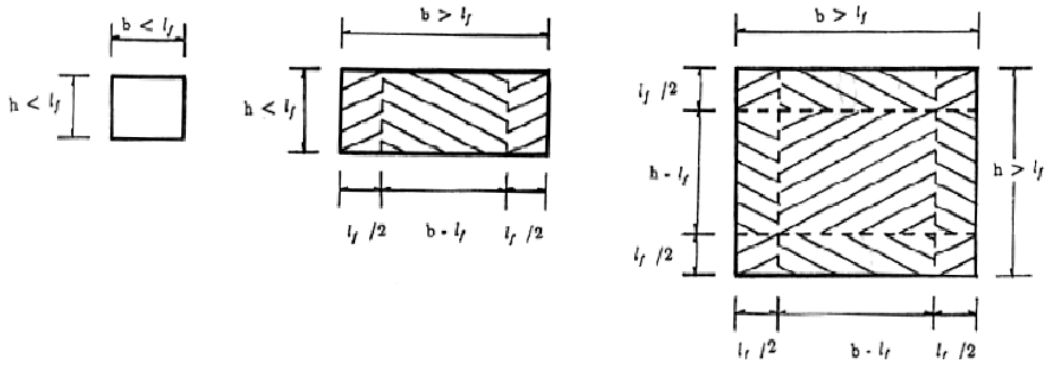

Figure 4.7 Different conditions with four boundaries (Soroushian, 1990).

Therefore, the tensile force at each layer of crack face of the beam can be obtained by multiplying the fiber force of that layer by the number of fibers. The force, f_i, of single fiber can be derived from the bond stress–slip relation mentioned in Equation 4.2.

4.3 Possibility of Pull Out

In fiber reinforced concrete the dimensions of the fibers vary from several millimeters to several centimeters. As the dimensions of the fibers get smaller, the possibility of fiber location crossing a crack at its full development length increases. Therefore, in addition to distribution and orientation of fibers, possibility of anchorage failure should be added to numerical study to obtain the failure mechanism (Oh, 2007). Figure 4.8 shows the relationship between fiber forces and probability of pull out failure. The development length, L_f, of a fiber for possibility of anchorage failure may be obtained as follows;

$$L_f = \frac{f_i}{F_{P\max}} \tag{4.4}$$

Where, F_{Pmax} is the maximum force carried by fiber before pull out failure. In order to avoid pull out (anchorage failure), the actual embedment length of fibers, L_f, should be larger than the required development length. Therefore, in this study, the probability of non-anchorage failure P_r is derived for two cases as follows:

- If the required fiber length is smaller than half of the fiber length;

$$P_r = 1 - \frac{L_f}{l_f} \tag{4.5}$$

- If the required fiber length is greater than half of the fiber length;

$$P_r = \frac{l_f}{4L_f} \tag{4.6}$$

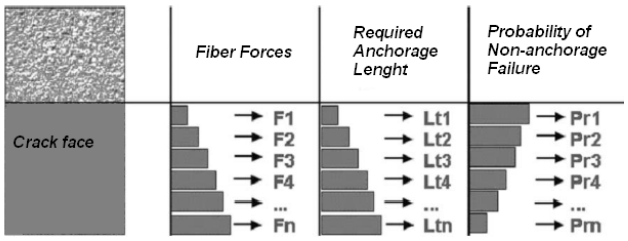

Figure 4.8 Probability of pull out failure(Oh, 2007).

Consequently, the tensile forces by fiber resistance to crack propagation can be lessened by multiplication with fiber orientation factor and probability of pull out failure.

4.4 Finite Element Analysis

SIF of concrete is assumed to be the fracture toughness criterion of concrete, and steel fibers give an additional preventative strength to fracture. In SIF calculations, concrete elements are selected as 8-node high-order elements and beam structure is assumed to be plane strain. To realize this, the crack path is separated into 10 layers. Flowchart of the program is presented in the Figure 4.9.

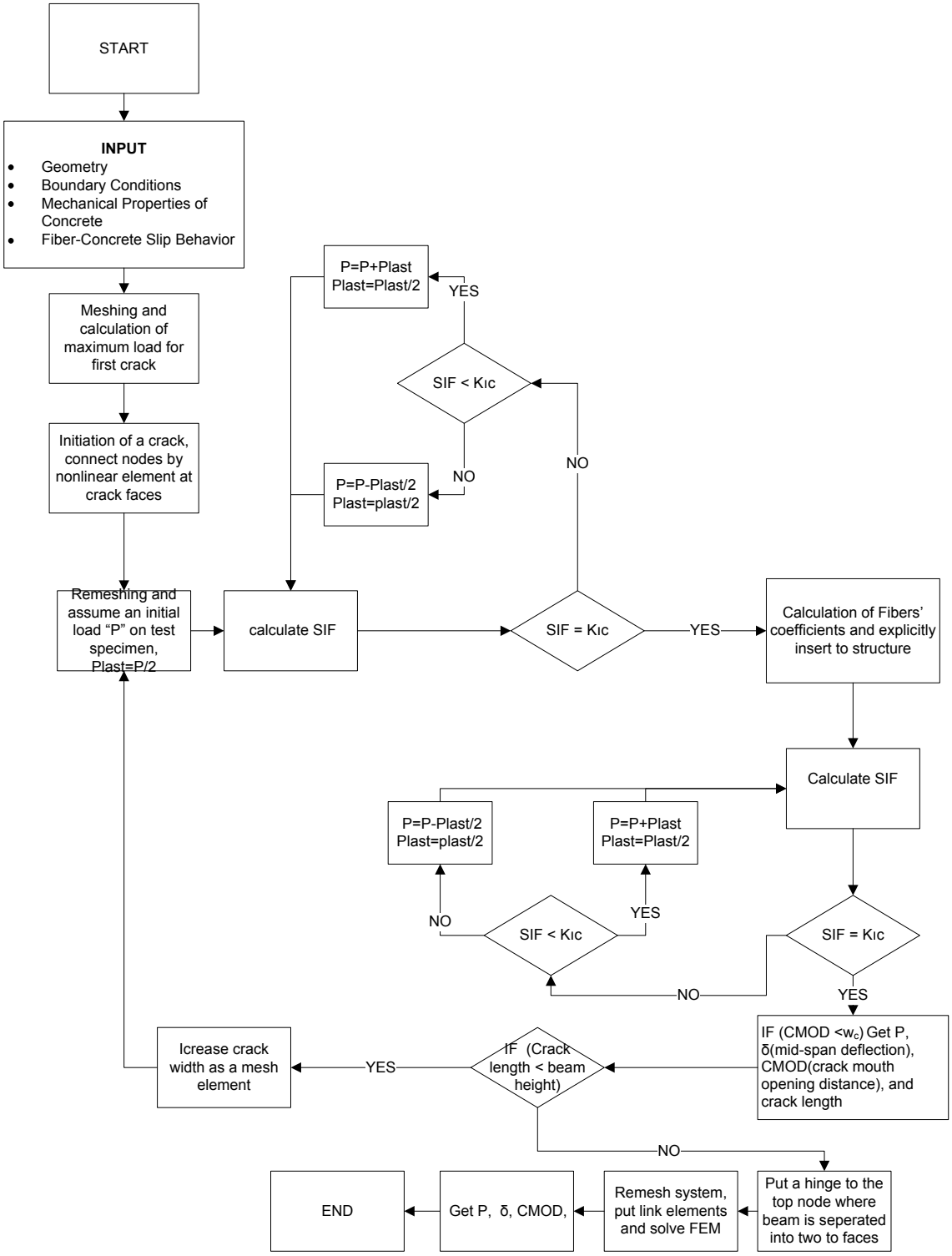

Figure 4.9 Flow chart for fracture process testing of steel fiber reinforced concrete.

Figure 4.10 illustrates some steps of the crack propagation process:

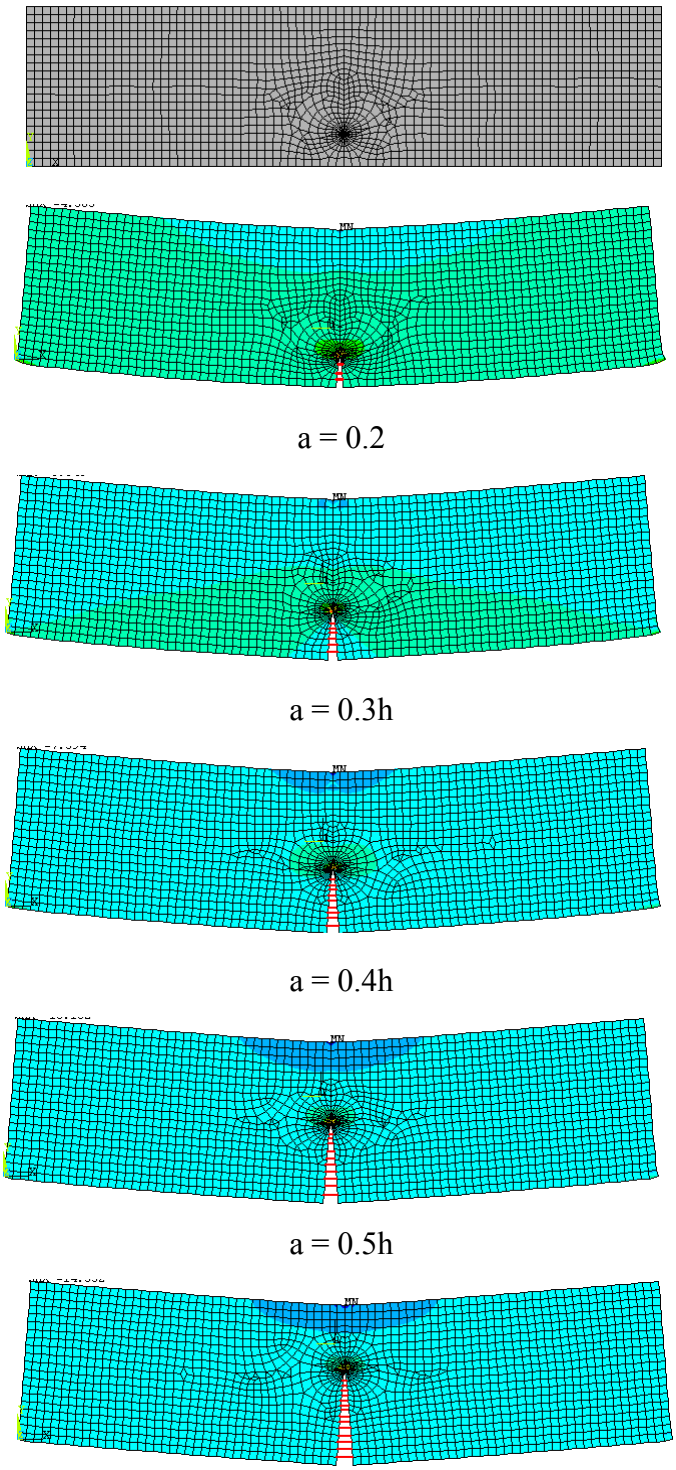

Figure 4.10 Crack Propagation Steps.

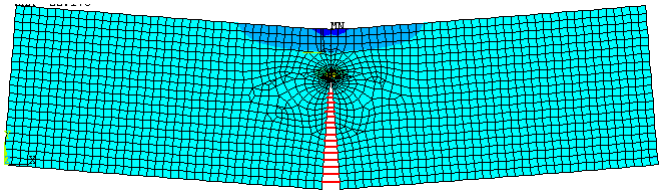

a = 0.7h

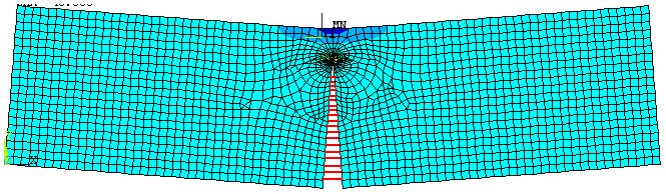

a = 0.8h

Figure 4.11 Crack Propagation Steps. (continued)

Consequently, the load–deflection curves are generated from the theory derived in this study by collecting critical forces, P_{cr}, and mid span displacement, δ, related to these loads. As it is mentioned earlier, data collected from numerical study are compared with the test data which are obtained by Oh's experimental study(Oh, 2007). The comparison between the two, for a fiber volume of 1.0% is presented in Figure 4.11.

Although it is assumed that crack occurs at only one point and it propagates in one direction, it can be seen in Figure 4.10 that the theoretical predictions agree with the test data even in post-cracking ranges. In other words, after the first crack is visible at the point where stress is equal to concrete ultimate tensile stress, the load starts to decrease with crack propagation until the fibers are able to carry the load on the beam. Figure 4.11b also presents a similar behavior of fiber reinforced concrete beam for a fiber volume of 1.5%.

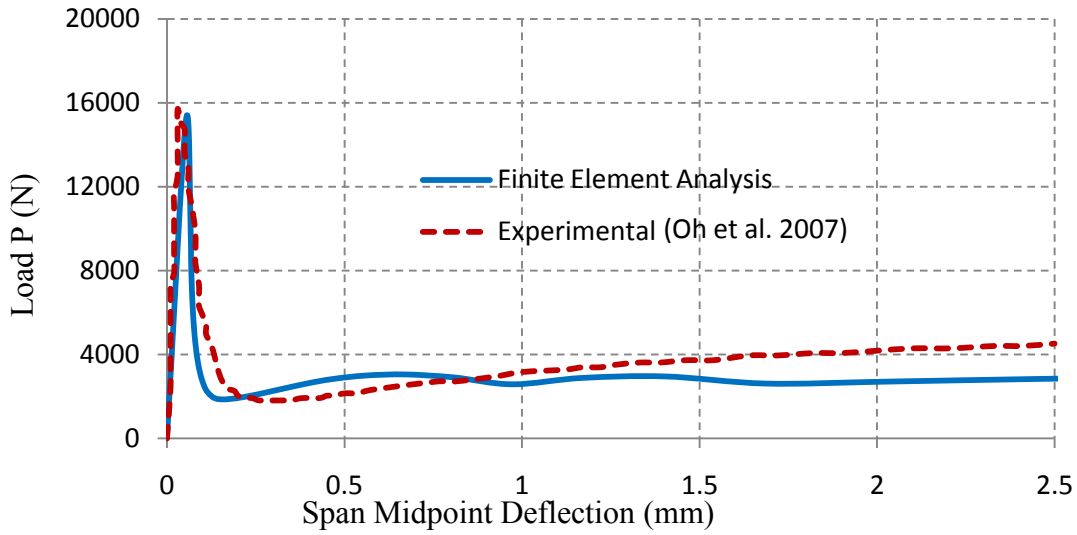

Figure 4.12 Load–deflection curves for fiber reinforced concrete beams V_f= 1.0.

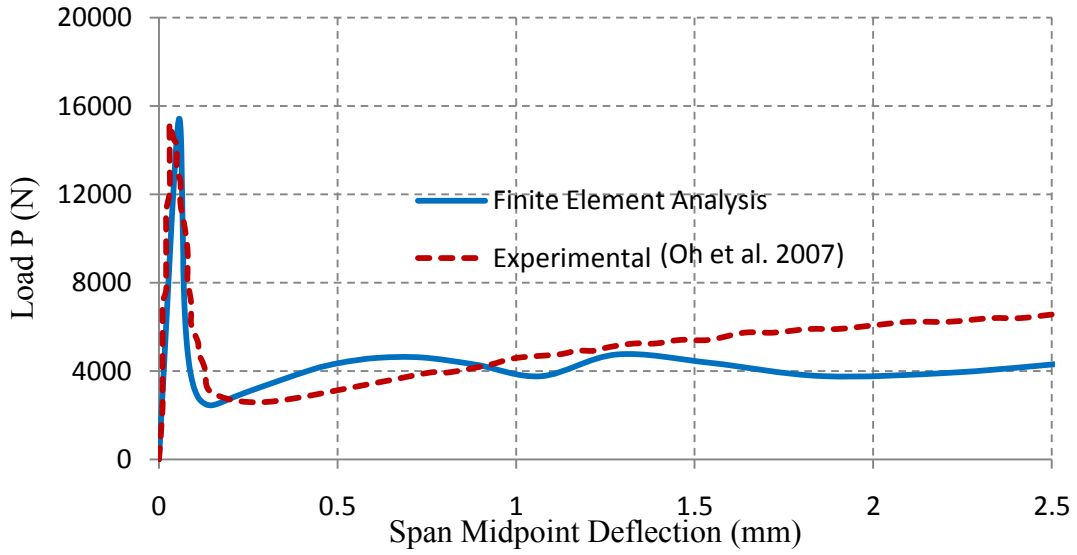

Figure 4.13 Load–deflection curves for fiber reinforced concrete beams V_f= 1.5.

Figure 4.13 shows the distinction between plain concrete and reinforced concrete with various contents of fibers. Obviously, there is a slightly difference between the curves until end of the crack propagation. Main reason of this phenomenon is that during crack propagation the crack opening distances are so small. Thus, forces carried by fibers are small. After concrete failure, fibers start to carry the loads. In contrary, in plain concrete after crack propagation reach to end layer, failure occurs as shown in Figures 4.13.

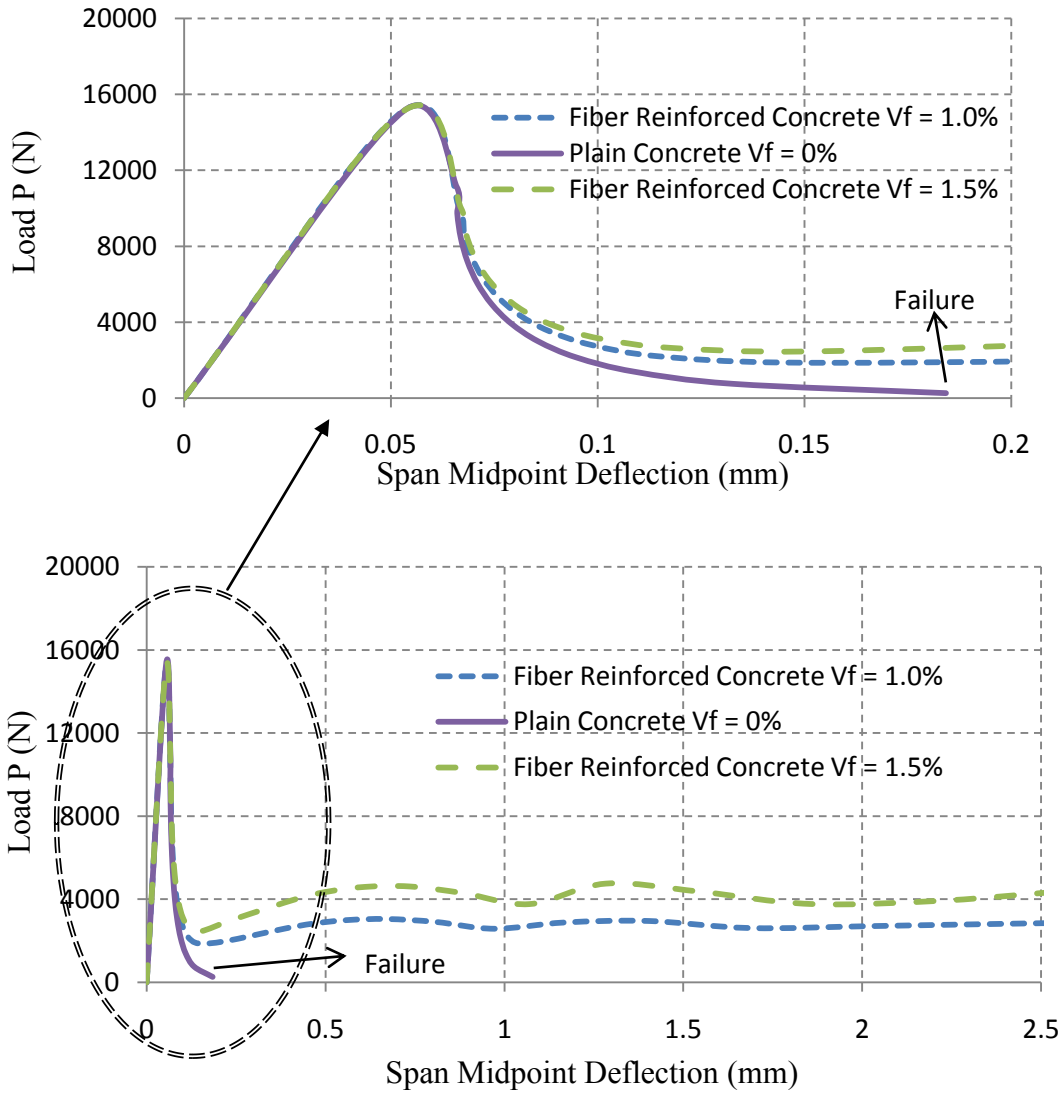

Figure 4.14 Load–deflection curve for fiber reinforced concretes and plain concrete

The proposed FE simulation platform could also be used to estimate the behavior of fiber reinforced concrete beams of varying fiber amounts. Figure 4.14 presents the comparison of load-deflection curves of beams with varying fiber amounts. From that figure it can be concluded that as the fiber volume increases the post cracking behavior of FRC beams completely changes and increase in the energy absorption capacity of beams is observed. However, in reality to produce FRC with higher fiber volume fractions is quite difficult. Therefore, it should be noted that FE solutions may lack those practical limitations.

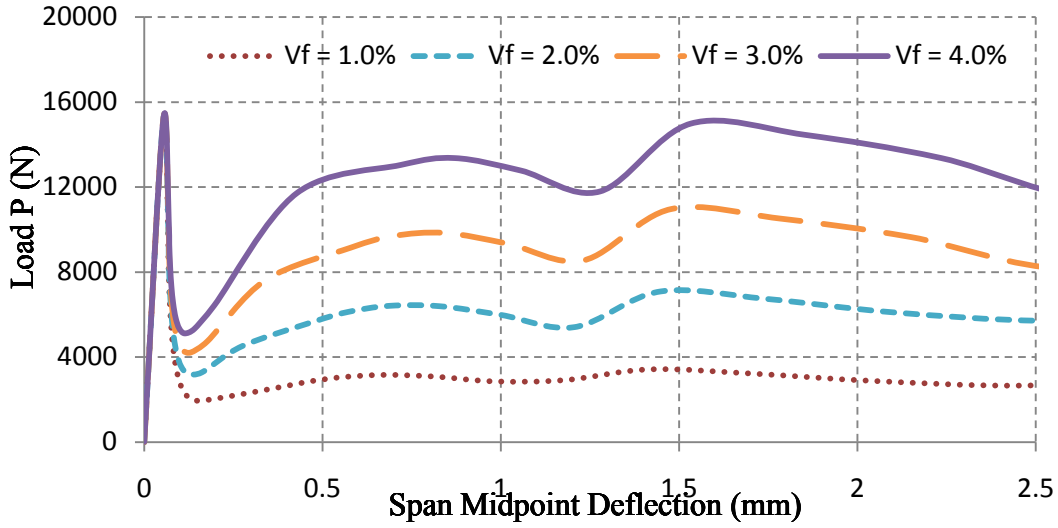

Figure 4.15 Load–deflection curve for various fiber contents.

CHAPTER 5

SUMMARY AND CONCLUSIONS

5.1 Summary

The purpose of the present study was to develop a finite element simulation tool for the fracture process of fiber reinforced concrete beam specimens subjected to flexural bending test. Therefore, the efficiency of mesh refinement has been presented in early chapters. Then, the slip-load mechanism of the fibers and their probabilities to resist tensile force are referenced. Unfortunately, since an experimental study is not presented in this thesis, Oh's experimental work is selected for the comparative part of the study (Oh B. H., 1992). Finally, two FE models and experimental work were used to verify the effect of steel fibers on fracture process and post process.

5.2 Conclusions

The following conclusions can be drawn from the results of this study:

1. As in all finite element calculations, mesh size and element type are the most important part of calculation. In FE model of fracture of concrete, if SIF or energy release rate is used as criterion on fracture, special elements must be used. Otherwise miscalculation and unexpected errors may come up. Therefore, 4-node elements should not be selected in this case. Additionally, mesh size and brittleness number should be considered for accurate results.

2. Even though fiber reinforced concrete is a nonlinear material, LEFM can be successfully used to predict its fracture behavior, and LEFM is an admissible application to predict reinforcement mechanism of fibers on the crack propagation process.

3. Probability of pull out mechanism of fibers from concrete matrix and orientation factors should be taken into account to obtain more accurate solutions.

4. The present study shows that the resisting load drops right after first cracking. As the fibers start to carry load at the crack plane, the resisting load starts to increase. The lowest resisting load at this point is increased by using high number of fibers.

5. Numerical methods presents that the toughness of concrete is enhanced with the addition of fibers into the matrix. On the other hand, a high volumetric ratio may affect the workability of concrete. Therefore, such simulation platforms should be used with care without ignoring practical limitations.

5.3 Recommendations for Future Studies

The FEM can be further utilized to answer other questions related with fracture mechanics of concrete. FE models of fracture process can be utilized depending on the problem under consideration. The following topics can be investigated:

1. The nonlinear effect of concrete during crack propagation is not included into the program. Future studies may take the nonlinearity of concrete into consideration.

2. In new generation finite element programs, there is special element which is called “Cohesive Zone Material”. These kinds of elements provide fracture debonding more easily. With this kind of modeling, fibers’ pull out mechanism of fibers in concrete may be directly introduced.

REFERENCES

ACI. (2009). Finite Element Analysis of Fracture in Concrete Structures. *ACI The 2009 Manual of Concrete Practice* , Part 5. 446.3R-97.

Anderson, T. L. (2005). *Fracture mechanics: fundamentals and applications.* CRC Press.

ANSYS, I. a. (2007, january). Programer's Manual for Ansys.

ANSYS, I. (2004). Documentation for ANSYS. Southpointe.

Araújo, T. B. (2000). Numerical estimation of fracture parameters in elastic and elastic-plastic analysis. *European Congress on Computational Methods in Applied Sciences and Engineering* , ECCOMAS, Barcelona.

ASTM. (2005). *Standard Method of Test for Plane-Strain Fracture Toughness of Metallic Material.* Mannual, American Society for Testing and Materials.

Banthia, N. T. (1994). Concrete reinforced with deformed steel fibers, part I: bond-slip mechanisms. *ACI Materials Journal* , 435-446.

Bažant, Z. P. (2002). Concrete Fracture Models: testing and practice. *Engineering Fracture Mechanics* , 165-205.

Bažant, Z. P. (1983). Crack Band Theory for Fracture Model for Concrete. *Materials and Structures, RIMEL, Vol. 6* , 155-177.

Bažant, Z. P. (1990). Determination of Fracture Energy, Process Zone Lenght and Brittleness Number from Size Effect, With application to rock and concrete. *Ineternational Journal of Fracture, Vol. 44* , 111-131.

Bažant, Z. P. (1976). Instability, Ductility and Size Effect in Strain-Softening Concrete. *J. Engineering Mechanics* , 331-334.

Bažant, Z. P. (1984). Size Effect in Blunt Fracture:Concrete, Rock, Metal. *Journal of Engineering Mechanics, ASCE, Vol.110, No. 4* , 518-535.

Bažant, Z. P.-G. (2002). Statistical prediction of fracture parameters of concrete and implications for choice of testing standard. *Cement and Concrete Research* , 529-556.

Carpinteri, A. P. (1992). Applications of Fracture Mechanics to Reinforced Concrete. *Elsevier Applied Science, London* , XIV + 616.

Carpinteri, A. P. (1999). Minimum Reinforcement in Concrete Science. *Oxford* , VUI + 203.

Carpinteri, A. P. (2007, 11 14). *Innovative Learning and Training on Fracture*. Retrieved from http://www.iltof.org/

Carpinteri, A. (1984). Stability of fracturing process in R.C. beams. *Journal of I Structural Engineering (ASCE), Vol. 110* .

Eftis, J. A. (1972). On the Modified Westergaard Equations for Certain Plane Crack Problems. *Int J. Fracture Mechanics* , 383-392.

Gopalaratman, V. S. (1985). Softening Response of Plain Concrete in Direct Tension. *ACI Journal , 82*, 310-323.

Hillerborg, A. M. (1976). Analysis of crack formation and crack growth in concrete by means of fracture mechanics and finite Elements. *Cement and Concrete Research, Vol 6, No 6* , 773-782.

Irwin, G. R. (1960). Plastic zone nera a Crack and Fracture Toughness. *in Proceeding of the Seventh Sagamore Ordnance MAterials Conference, Syracuse University* , IV-60.

Jenq, Y. S. (1985). A Two Parameter Fracture Model for Concrete. *Journal of Engineering Mechanics, Vol.111, No. 4* , 1227-1241.

Jenq, Y. S. (1985). Two parameter fracture model for concrete. *J. Eng. Mech.* , 1227-1241.

Kaplan, M. F. (1961). Crack propagation and the fracture of concrete. *ACI journal* , 591-610.

Karihaloo, B. N. (1989). An improved effective crack model for the determination of fracture toughness of cocnrete. *Cem. Concr. Res.* , 603-610.

Kesler, C. N. (1972). Fracture mechanics-its applicability to concret, Proceedings of the International Conference on the Mechanical Behaviour of Materials. *Society of Materials Science* , 113-124.

Kim J.H., P. G. (2002). Mixed-mode Fracture of Orthotropic Functionally Graded Materials Using Finite Elements and the Modified Crack Closure Method. *Engineering Fracture Mechanics* , Vol. 69 1557-1586.

Oh, B. H. (1992). Flexural analysis of reinforced concrete beams containing steel fibers. *ASCE J Structral Engineering* , 118(10):2691–8.

Oh, B. H. (2007). Fracture behavior of concrete members reinforced. *Engineering Fracture Mechanics* , 243–257.

Planas, J. E. (1992). Fracture Criteria for Concrete: Mathematical Approximations and Experimental Validation. *35*, 87-94.

Rashid, Y. R. (1968). Ultimate Strength Analysis of Presetressed Concrete Pressure Vessels . *Nuclear Engineeering and Design* , 379-386.

Rice, J. R. (1968). A Path Independent and the approximate analysis of strain concentration by notches and cracks. *Journal of Applies Mechanics* , 379-286.

Robert D. Cook, D. S. (2001). *Concept and Applications of Finite Element Analysis.* Madison: Wiley.

Sanford, R. J. (1979). Acritical Re-examination of the Westergaard Method for Solving Opening-Mode Crack Problems. *Mechanics Research Communications* , 289-294.

Sanforld, R. J. (2002). *Principles of Fracture Mechanics.* Prentice Hall.

Shah, S. P. (1995). *Fracture Mechanics of Concrete, Applications of Fracture Mechanics to Concrete, Rock and Other Quasi-Brittle Materials.* NY: A Wiley-Interscience Publication.

Soroushian, P. L. (1990). Distribution and orientation of fibers in steel fiber reinforced concrete. *ACI Materials Journal* , 433–442.

Tada, H. P. (1985). The Stress Analysis of Cracks Handbook. *Paris Productions Inc (Del Res. Corp.), St. Louis* .

Wells, A. A. (1961). Unstable Crack Propagation in Metals: Cleavage and Fast Fracture. *Process of Cracfield Crack Propagation Symposium* , 210-230.

APPENDIX A

MESH RESOLUTIONS

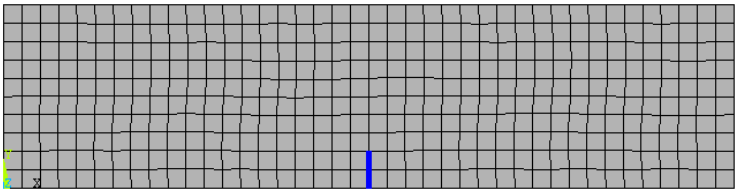

a) a/W=0.2

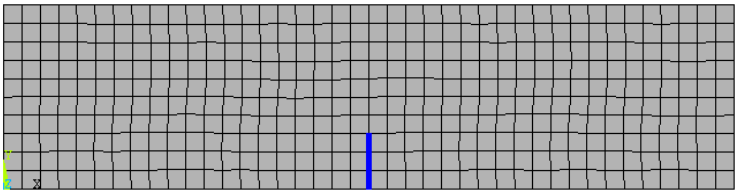

b) a/W=0.3

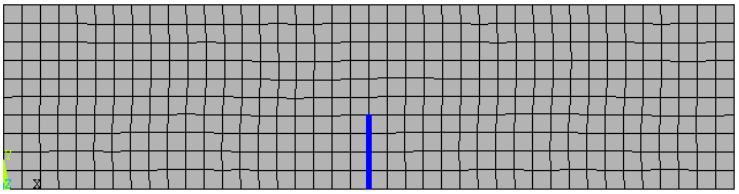

c) a/W=0.4

Figure A.8.1 Mesh resolution according to 10 elements at fracture surface.

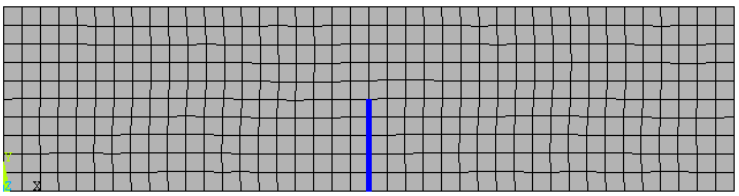

d) a/W=0.5

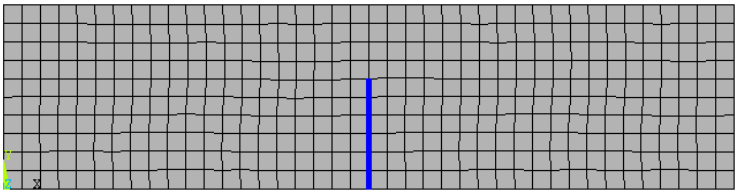

e) a/W=0.6

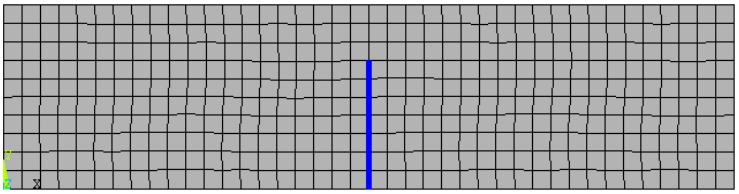

f) a/W=0.7

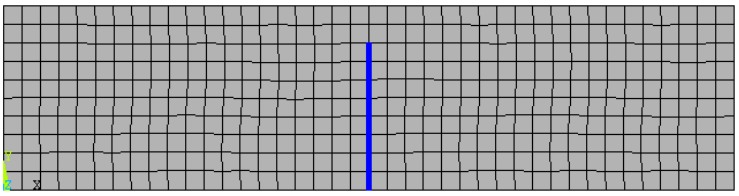

g) a/W=0.8

Figure A.1 Mesh resolution according to 10 elements at fracture surface. (Continued)

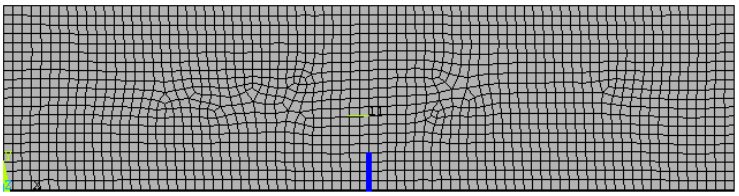

a) a/W=0.2

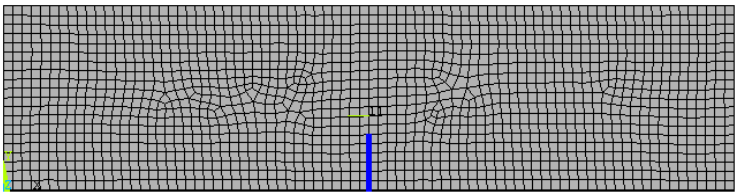

b) a/W=0.3

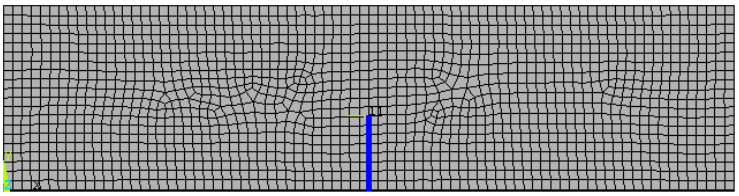

c) a/W=0.4

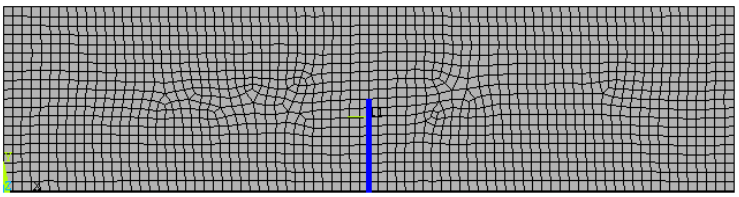

d) a/W=0.5

Figure A.2 Mesh resolution according to 20 elements at fracture surface.

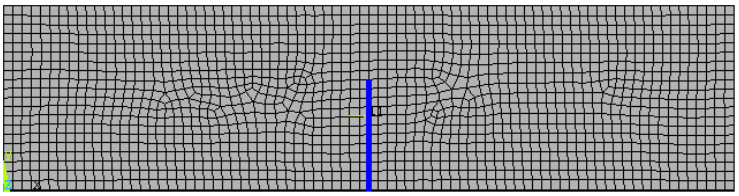

e) a/W=0.6

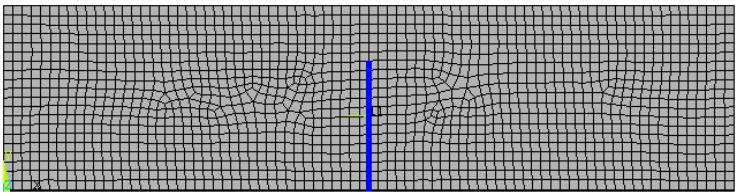

f) a/W=0.7

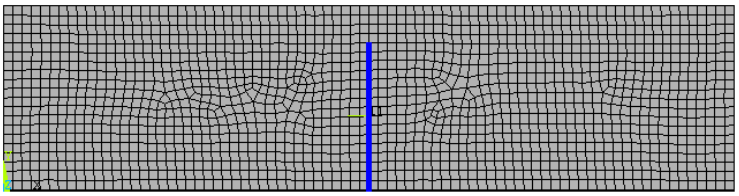

g) a/W=0.8

Figure A.2 Mesh resolution according to 20 elements at fracture surface. (Continued)

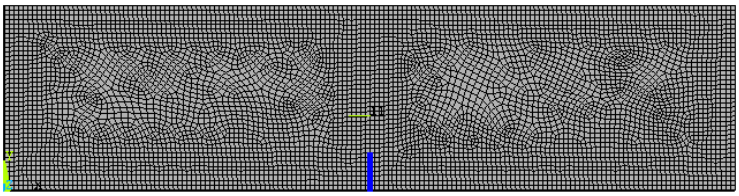

a) a/W=0.2

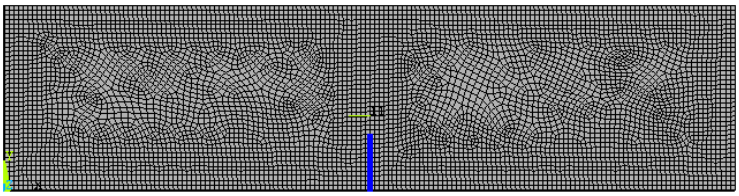

b) a/W=0.3

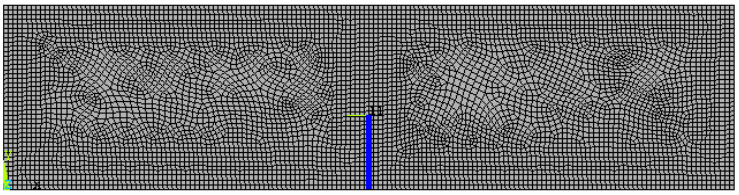

c) a/W=0.4

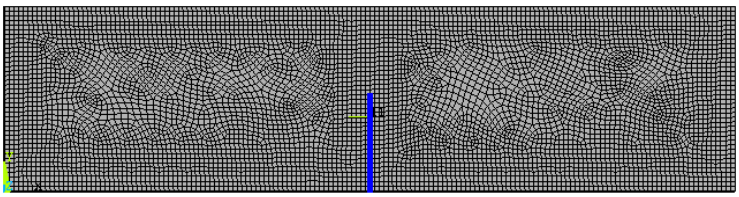

d) a/W=0.5

Figure A.3 Mesh resolution according to 40 elements at fracture surface.

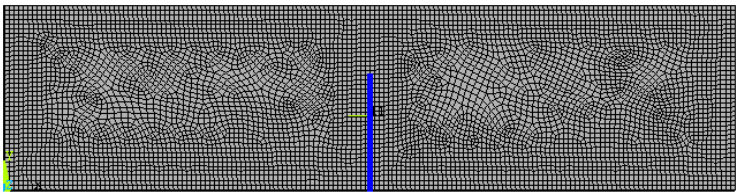

e) a/W=0.6

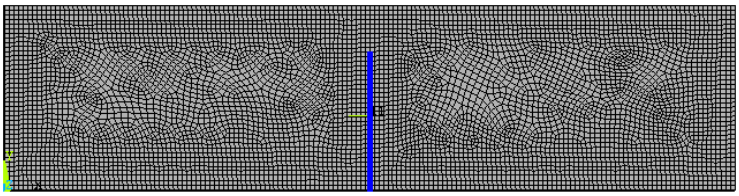

f) a/W=0.7

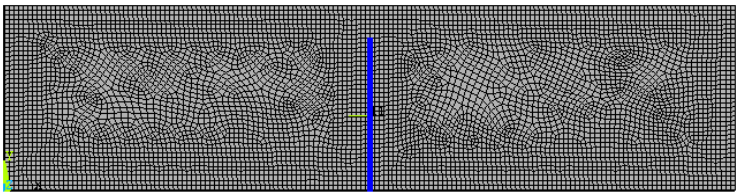

g) a/W=0.8

Figure A.3 Mesh resolution according to 40 elements at fracture surface. (Continued)

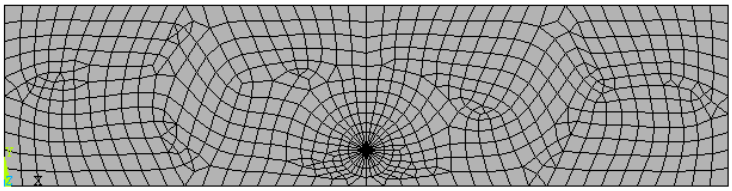

a) a/W=0.2

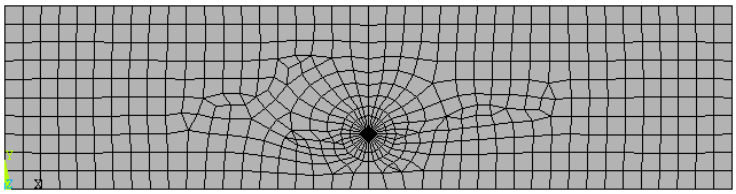

b) a/W=0.3

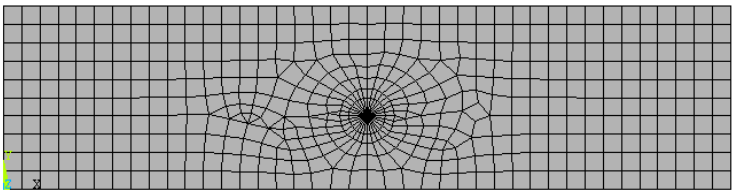

c) a/W=0.4

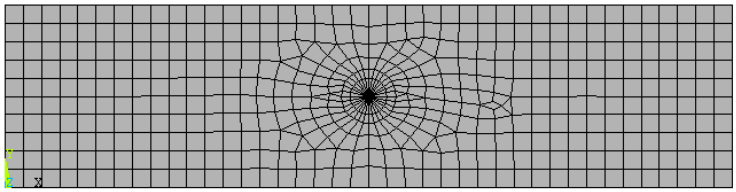

d) a/W=0.5

Figure A.4 Mesh resolution according to 13 elements at fracture surface.

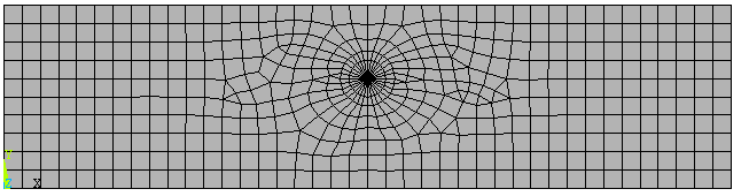

e) a/W=0.6

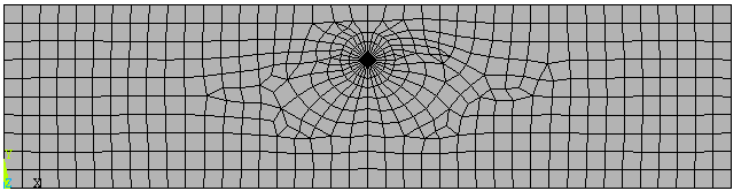

f) a/W=0.7

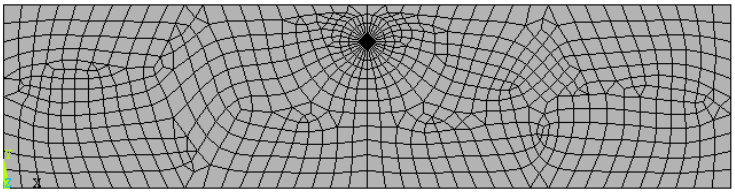

g) a/W=0.8

Figure A.4 Mesh resolution according to 13 elements at fracture surface. (Continued)

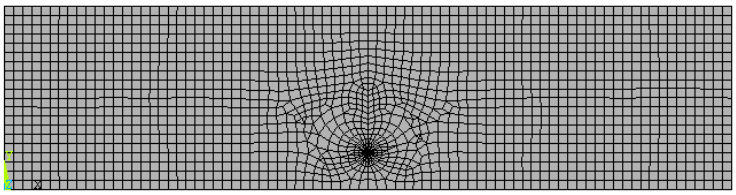

a) a/W=0.2

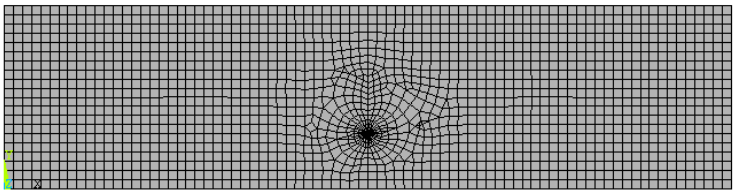

b) a/W=0.3

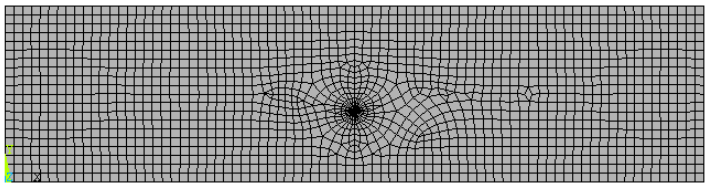

c) a/W=0.4

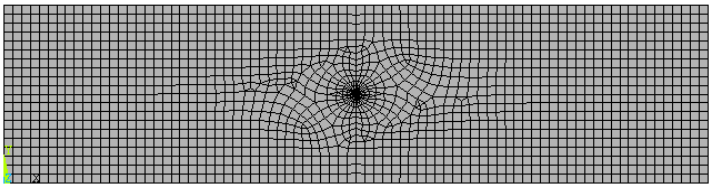

d) a/W=0.5

Figure A.5 resolution according to 23 elements at fracture surface.

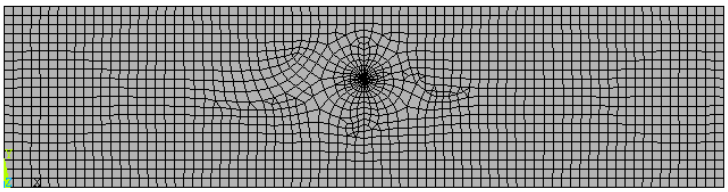

e) a/W=0.6

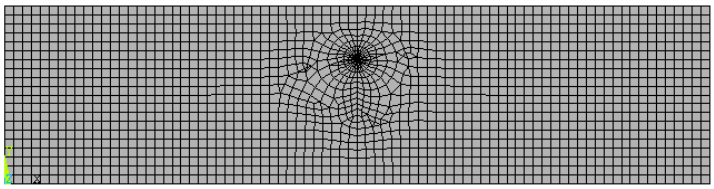

f) a/W=0.7

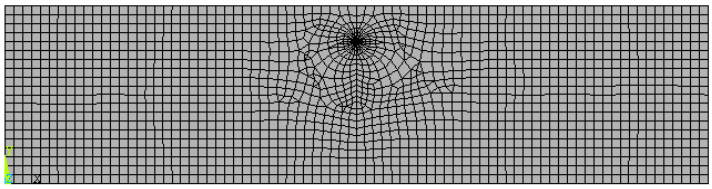

g) a/W=0.8

Figure A.5 Mesh resolution according to 23 elements at fracture surface. (Continued)

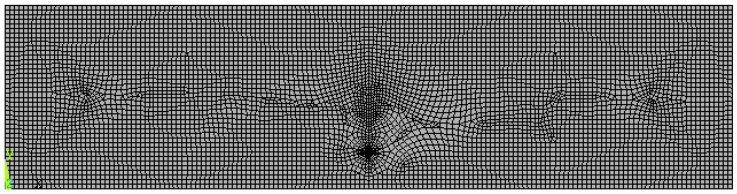

a) a/W=0.2

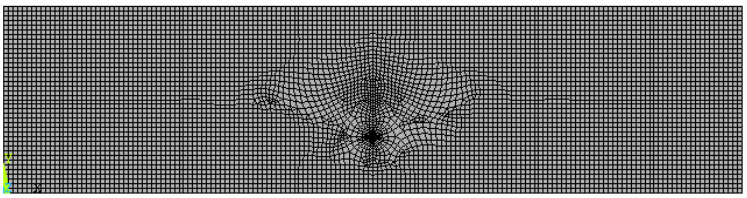

b) a/W=0.3

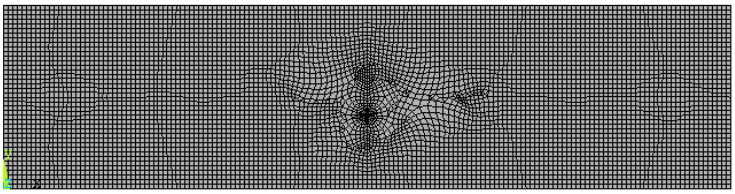

c) a/W=0.4

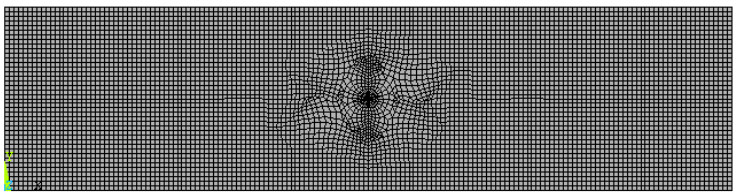

d) a/W=0.5

Figure A.6 Mesh resolution according to 43 elements at fracture surface.

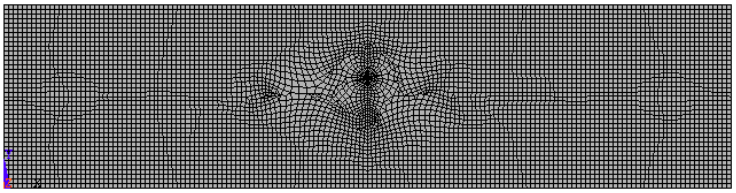

e) a/W=0.6

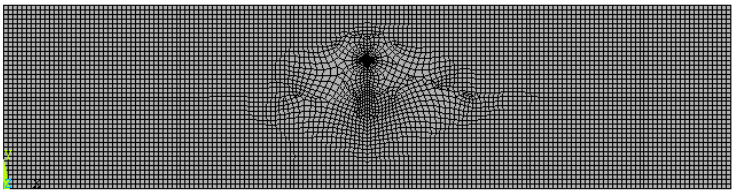

f) a/W=0.7

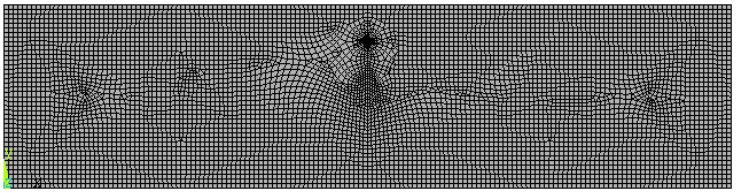

g) a/W=0.8

Figure A.6 Mesh resolution according to 43 elements at fracture surface. (Continued)